NASA/CR—2003-212529 ARL–CR–0531

Simulating Fatigue Crack Growth in Spiral Bevel Pinion

Ani Ural, Paul A. Wawrzynek, and Anthony R. Ingraffea
Cornell University, Ithaca, New York

August 2003

The NASA STI Program Office . . . in Profile

Since its founding, NASA has been dedicated to the advancement of aeronautics and space science. The NASA Scientific and Technical Information (STI) Program Office plays a key part in helping NASA maintain this important role.

The NASA STI Program Office is operated by Langley Research Center, the Lead Center for NASA's scientific and technical information. The NASA STI Program Office provides access to the NASA STI Database, the largest collection of aeronautical and space science STI in the world. The Program Office is also NASA's institutional mechanism for disseminating the results of its research and development activities. These results are published by NASA in the NASA STI Report Series, which includes the following report types:

- TECHNICAL PUBLICATION. Reports of completed research or a major significant phase of research that present the results of NASA programs and include extensive data or theoretical analysis. Includes compilations of significant scientific and technical data and information deemed to be of continuing reference value. NASA's counterpart of peer-reviewed formal professional papers but has less stringent limitations on manuscript length and extent of graphic presentations.

- TECHNICAL MEMORANDUM. Scientific and technical findings that are preliminary or of specialized interest, e.g., quick release reports, working papers, and bibliographies that contain minimal annotation. Does not contain extensive analysis.

- CONTRACTOR REPORT. Scientific and technical findings by NASA-sponsored contractors and grantees.

- CONFERENCE PUBLICATION. Collected papers from scientific and technical conferences, symposia, seminars, or other meetings sponsored or cosponsored by NASA.

- SPECIAL PUBLICATION. Scientific, technical, or historical information from NASA programs, projects, and missions, often concerned with subjects having substantial public interest.

- TECHNICAL TRANSLATION. English-language translations of foreign scientific and technical material pertinent to NASA's mission.

Specialized services that complement the STI Program Office's diverse offerings include creating custom thesauri, building customized databases, organizing and publishing research results . . . even providing videos.

For more information about the NASA STI Program Office, see the following:

- Access the NASA STI Program Home Page at ***http://www.sti.nasa.gov***

- E-mail your question via the Internet to help@sti.nasa.gov

- Fax your question to the NASA Access Help Desk at 301–621–0134

- Telephone the NASA Access Help Desk at 301–621–0390

- Write to:
  NASA Access Help Desk
  NASA Center for AeroSpace Information
  7121 Standard Drive
  Hanover, MD 21076

NASA/CR—2003-212529 ARL–CR–0531

Simulating Fatigue Crack Growth in Spiral Bevel Pinion

Ani Ural, Paul A. Wawrzynek, and Anthony R. Ingraffea
Cornell University, Ithaca, New York

Prepared under Contract NAS3–1993

National Aeronautics and
Space Administration

Glenn Research Center

August 2003

The Propulsion and Power Program at
NASA Glenn Research Center sponsored this work.

Available from

NASA Center for Aerospace Information
7121 Standard Drive
Hanover, MD 21076

National Technical Information Service
5285 Port Royal Road
Springfield, VA 22100

Available electronically at http://gltrs.grc.nasa.gov

1. Introduction

This project investigates computational modeling of fatigue crack growth in spiral bevel gears. Current work is a continuation of the previous efforts made to use the Boundary Element Method (BEM) to simulate tooth-bending fatigue failure in spiral bevel gears. This report summarizes new results predicting crack trajectory and fatigue life for a spiral bevel pinion using the Finite Element Method (FEM).

Predicting crack trajectories is important in determining the failure mode of a gear. Cracks propagating through the rim may result in catastrophic failure, whereas the gear may remain intact if one tooth fails and this may allow for early detection of failure. Being able to predict crack trajectories is insightful for the designer. However, predicting growth of three-dimensional arbitrary cracks is complicated due to the difficulty of creating three-dimensional models, the computing power required, and absence of closed-form solutions of the problem.

Previously in this project, tooth-bending fatigue failure in spiral bevel gears was investigated using the BEM [1]. These analyses were significant in developing a method for predicting three-dimensional, non-proportional, fatigue crack growth incorporating moving loads. Prior to the BEM study, there were not many examples of three-dimensional crack growth work on gears. Most of the gear studies in the literature are two-dimensional analyses. Furthermore, moving loads had not been considered in these analyses.

The BEM predictions were helpful to determine areas in need of further research. These were: improving accuracy of simulation by switching from the boundary element to the finite element method, decreasing computation time by employing parallel FEM analysis, and improving modeling of contact tooth loads.

Substantial improvement in computation time has been achieved by using parallel FEM technologies on PC-clusters. This makes it possible to simulate crack growth in large models, like the current gear problem, in a few minutes. It is also possible to obtain accurate values of stress intensity factors (SIF) using the FEM and elastic, equivalent domain J-integral approaches. A new technique was developed for modeling moving tooth loads, which decreases the computation time while introducing a more efficient procedure for applying contact loads.

Another focus of this project was performing three-dimensional contact analysis of a spiral bevel gear set incorporating cracks. These analyses were significant in determining the influence of change of tooth flexibility due to crack growth on the magnitude and location of contact loads. This is an important concern since change in contact loads might lead to differences in SIFs and therefore result in alteration of the crack trajectory.

Contact analyses performed in this report showed the expected trend of decreasing tooth loads carried by the cracked tooth with increasing crack length. Decrease in tooth loads lead to differences between SIFs extracted from finite element contact analysis and finite element analysis with Hertz contact loads. This effect became more pronounced as the crack grew.

2. Three-dimensional FEM Simulations of Fatigue Crack Growth in Spiral Bevel Gears

The main objective of the current work is to demonstrate that we can improve accuracy and efficiency of crack growth simulations in spiral bevel pinion through FEM computations along with improved modeling of tooth loads. In the current study, as in previous BEM simulations, LEFM theories are used for fatigue crack growth predictions in gears. Fatigue crack growth rates were determined using a modified Paris model accounting for crack closure. Crack trajectory predictions are made using the maximum circumferential stress theory. Moving loads were taken into account by discretizing the loading into 15 steps that created a non-proportional load history at the tooth root.

Accuracy of computations can be improved using the FEM that allows a better SIF calculation method, the equivalent domain J-integral method. Solution time for each load step can be decreased substantially by employing parallel FEM analysis. Another improvement in the accuracy of the results can be obtained by developing a better representation of moving contact loads. This is accomplished by approximating the moving contact ellipse by interpolation using the shape functions on the surfaces of the loaded elements. In the earlier boundary element computations, contact ellipses were a part of the geometry models. Since the ellipses overlapped, four different geometry models were needed for each crack configuration. In the current approach, contact loads are no longer a part of the geometry model. This approach brings a substantial decrease in computation time since only one geometry model for each crack configuration is now needed.

The method used in FEM simulations of spiral bevel gear is composed of the following steps:

1. Create initial geometry model of the spiral bevel pinion using OSM.
2. Specify boundary conditions and material properties in FRANC3D.
3. Initiate crack in FRANC3D.
4. Create a surface mesh composed of triangular elements in FRANC3D.
5. Create a 3D FEM mesh of the model composed of tetrahedra by J-Mesh using a geometry description file written out from FRANC3D.
6. Calculate the magnitude and location of the nodal contact loads for each load step on the loaded elements using the mesh file produced by J-Mesh.
7. Run FEM analysis on a parallel PC-cluster for 15 discrete load steps. Using the displacement results, calculate SIF values at each discrete crack front point for each load step.
8. Calculate the amount of crack extension at each discrete crack front point as a result of 15 steps of non-proportional moving load.
9. Determine new crack front by piecewise least squares fit of the propagated points corresponding to each discrete crack front point in FRANC3D.
10. Remesh surface locally and repeat steps 5 to 10.

2.1 Modeling of Moving Tooth Loads

Contact in a spiral bevel gear occurs in three-dimensions following a path along the tooth surface starting from the fillet of the toe to the top of the heel. In analyzing the spiral bevel gear, it is assumed that the contact between the gear and pinion follows Hertz theory of elastic contact. Hertzian contact holds as long as the significant dimensions of the contact area are small compared to the dimensions of each body and to the relative radii of curvature of surfaces [2]. Hertz theory assumes that surfaces are continuous and non-conforming, strains are small, each solid can be considered as an elastic half-space and surfaces are frictionless.

Under these assumptions, only normal pressure acts between two bodies due to Hertz contact producing normal displacements of the surfaces. Since the contact area is assumed to be elliptical the region is defined by,

$$\frac{x^2}{a^2}+\frac{y^2}{b^2}=1 \tag{1}$$

with semi-ellipsoidal pressure distribution of the form,

$$p = p_0\left(1-\frac{x^2}{a^2}-\frac{y^2}{b^2}\right)^{1/2} \tag{2}$$

Total load acting on the ellipse and average load are then calculated as,

$$p=\frac{2\pi ab}{3}p_0\ ,\quad p_{avg}=\frac{2}{3}p_0 \tag{3}$$

In the above equations p_0 denotes the Hertz stress which is the maximum stress, a and b are half of major and minor axes of the ellipse, respectively, Figure 2.1.

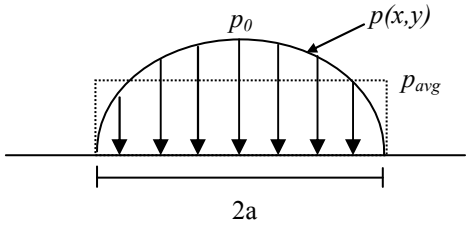

Figure 2.1: Representation of Hertz stress over an elliptical area.

In order to determine the contact points on the gear tooth, the method described in [3] is used to map the three-dimensional contact path into a two dimensional space. The following equations were used for the transformation:

$$\begin{aligned} R_{N,M,1,2} &= (X_{N,M,1,2}{}^2 + Y_{N,M,1,2}{}^2)^{1/2} \\ \xi_N &= (Z_N - Z_M)\cos\alpha + (R_N - R_M)\sin\alpha \\ \eta_N &= (R_N - R_M)\cos\alpha + (Z_N - Z_M)\sin\alpha \\ \sin\alpha &= \frac{R_1 - R_2}{2a} \qquad \cos\alpha = \frac{Z_1 - Z_2}{2b} \end{aligned} \tag{4}$$

X_M, Y_M, Z_M = coordinates of mean contact point (corresponds to the contact ellipse centers)
X_N, Y_N, Z_N = coordinates of an arbitrary contact point
$X_{1,2}, Y_{1,2}, Z_{1,2}$ = coordinates of points corresponding to 1 and 2 in Figure 2.2 in three dimensions.

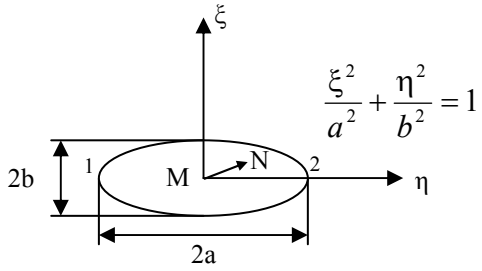

Figure 2.2: Sketch of transformed contact ellipse with mean contact point M and an arbitrary contact point N.

An algorithm was developed to find the nodes within the contact ellipses and to calculate the applied load on these nodes. This algorithm:

1. reads the nodal information from the mesh and geometry files created by 3D FEM meshing program,
2. retrieves the geometry information of the *n* th contact ellipse,
3. transforms the nodal points defined in 3D coordinates into contact plane,
4. checks if the mesh nodes are within the contact area bounded by the *n* th ellipse (*n* = 1…15), eg. Figure 2.3,
5. calculates nodal contact loads if the node is within the contact area, and
6. writes out the information of nodes found by this search and corresponding loads.

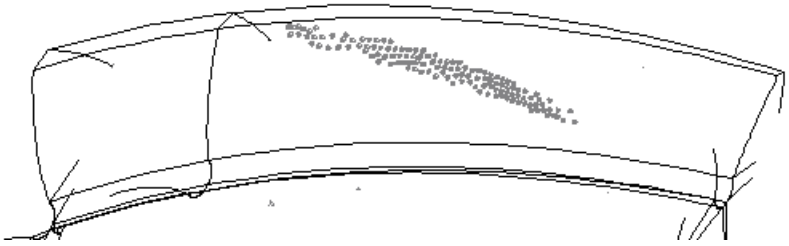

Figure 2.3: Nodal points where contact loads are applied for load step 11.

2.2 Parallel FEM

Understanding fracture phenomena in materials is crucial for science and engineering applications such as crack propagation in spiral bevel gears. However, crack growth simulations are complicated and computationally expensive in realistic structures. In order to solve realistic 3D problems, it is necessary to develop fast and accurate computational simulation tools.

The BEM is an alternative to the FEM for solving large problems. The BEM is advantageous since it only requires a surface mesh and has fewer equations to be solved. However, it entails a fully dense, nonsymmetric system of equations, and it is difficult to extract accurate near-crack-front stresses and displacements. In this respect, it is more desirable to use FEM. This brings the challenge of implementing fast and robust parallel sparse solvers.

A parallel PC-cluster in Cornell Theory Center was used for the development of a parallel FEM solver for crack growth simulations. The hardware consists of 32 nodes of a 64 node cluster of Dell PowerEdge 1650 servers with a Giganet interconnect running Microsoft Windows 2000 Advanced Server. Each node contains 2 Intel Pentium III processors clocked at 1 GHz and 2 GB of RAM. Only one processor per node is used for the simulations.

Parallel FEM simulation of crack propagation makes it possible to simulate large problems that were impossible or impractical to solve previously. The objective in developing such a system is to be able to solve a real-life problem with multiple crack propagation steps with 1,000,000 degrees of freedom in an hour. Such a problem with 10,000 degrees of freedom takes about 100 hours using a state-of-the-art single processor workstation [4].

Crack propagation in a spiral bevel gear stands as a large, realistic engineering problem that incorporates the computational difficulties mentioned above. In that respect, the development of parallel FEM simulations is a significant step in achieving the goal of developing a practical and accurate numerical design tool for gears.

2.3 SIF Calculations

Complex problems, such as the current gear problem, require computation of mixed mode SIFs due to the combined loading that they receive. In the literature, several approaches for computing SIFs can be found. Among these methods, the displacement correlation method [5-8] and equivalent domain J-integral methods [9-14] are widely used in numerical computations.

In the previous BEM simulations of the spiral bevel gear, the displacement correlation method was used for calculating SIFs. This method only requires displacement information on the boundary near the crack front and is computationally efficient. Since BEM solves for displacement information only on the boundaries, this method is suitable for the BEM analysis. The displacement correlation method makes use of numerical solutions for displacements in combination with the analytic solutions of SIFs. This method is only as accurate as the computed displacements at the correlation points.

The equivalent J-integral method is adaptable to complex problems and presents much more flexibility in the type of applications for which it can be used. We used the equivalent domain J-integral approach instead of displacement correlation in the FEM simulations of the spiral bevel gear.

J-integral is the energy release expression associated with crack growth defined as an integral along a contour that encloses a crack tip. J-integral is defined as [15],

$$J = \int_{\Gamma} (Wn_1 - \sigma_{ij} \frac{\partial u_i}{\partial x_1} n_j) d\Gamma \tag{5}$$

where W is the strain energy density, n_j is the unit outward normal to the contour, σ_{ij} is the traction exerted on the body enclosed by Γ and crack surface. This integral is evaluated along an arbitrary contour enclosing the crack tip and is path independent.

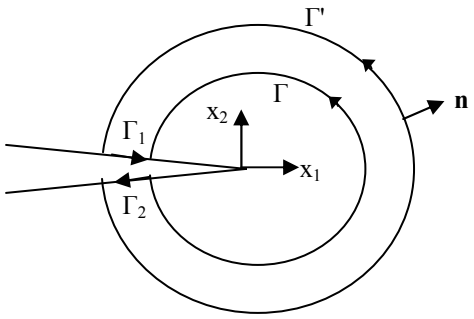

$$\Gamma_T = \Gamma' + \Gamma_1 + \Gamma_2 + \Gamma$$

Figure 2.4: Paths of J-integral calculations at a crack tip.

Numerical evaluation of the J-integral involves the use of equivalent domain integral approach. In this approach, the integration along the contour is replaced by an integral over a finite size domain. The expression for J-integral then becomes,

$$J_k = \int_{\Gamma_T} [W\delta_{kj} - \sigma_{ij} \frac{\partial u_i}{\partial x_k}] n_j q dA \qquad k=1,2. \tag{6}$$

A continuous function $q(x_1,x_2)$ is introduced in the above equation in order to replace the integration contour Γ by Γ_T. Function q has a unit value at the crack tip and it is zero along Γ', Γ_1 and Γ_2. The variation of this function within the domain is arbitrary. Using divergence theorem equation 6 takes the form,

$$J_k = \int_{\Gamma_T} [W \frac{\partial q}{\partial x_k} - \sigma_{ij} \frac{\partial u_i}{\partial x_k} \frac{\partial q}{\partial x_j}] dA - \int_{\Gamma_T} \{\frac{\partial W}{\partial x_k} - \frac{\partial}{\partial x_j} [\sigma_{ij} \frac{\partial u_i}{\partial x_k}]\} q dA \tag{7}$$

Note that the second term of this integral vanishes for elastic problems. SIFs are calculated within the vicinity of the 3D crack front by the pointwise values of J-integral. 3D cracks can be represented by 2D plane strain fields at the crack front points. These fields are satisfied only within close proximity of the crack tip, however it is well known that finite element calculations of the field quantities are not very accurate close to the crack tip. Equivalent domain integral approach circumvents this difficulty by replacing the line integral by a finite domain integral. The relation between the J-integral and SIFs is given for an isotropic, linear elastic material as follows,

$$J_1 = \frac{\kappa+1}{8G}(K_I^{\,2} + K_{II}^{\,2}) \quad \text{and} \quad J_2 = -\frac{2(\kappa+1)}{8G} K_I K_{II} \tag{8}$$

In the above equations J_2 is not path independent. For a pure mode I or mode II problem, SIFs can be calculated directly from these equations however under mixed mode loading K_I and K_{II} cannot be calculated separately. Bui [16] proposed a mixed mode separation method by decomposing the elastic displacement field into symmetrical and anti-symmetrical parts. This results in separation of J into two components that are given as follows [16],

$$J = J_1 + J_2 \ , \quad J_I = \frac{1-\nu^2}{E} K_I^{\,2} \ , \quad J_{II} = \frac{1-\nu^2}{E} K_{II}^{\,2} \ , \quad u_i = u_i^{\,I} + u_i^{\,II} \tag{9}$$

Examples of numerical investigations on mixed mode problems using this approach yielded highly accurate results [17,18].

Numerical techniques generally provide good results in an average sense over the domain. However, governing equations and/or boundary conditions are only approximately satisfied at any one point. This indicates that displacement correlation SIFs are not very accurate since they depend on the displacement values at a point. On the other hand, J-integral SIFs give better results due to considering much more of the results domain over which approximation errors tend to cancel.

Two models with known analytic solution are investigated to show the higher accuracy of the FEM calculations. The first model is a single, internal, flat, penny-shaped crack in an infinite body. The radius of the penny-shaped crack is 0.1. This crack is centered in a block with dimensions 10 x 5 x 5.

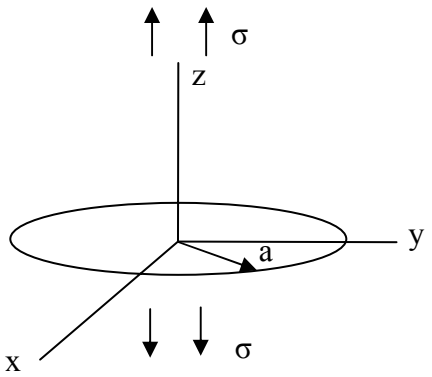

Figure 2.5: Flat, internal penny-shaped crack subjected to remote tension.

For this problem Mode II and Mode III SIFs are zero. The analytical solution for the Mode I SIF is given by [19],

$$K_I = 2\sigma\sqrt{\frac{a}{\pi}} \tag{10}$$

Table 2.1 shows the comparison of solutions from the BEM, and FEM and the analytical solution. BEM results shown in Table 2.1 are calculated by the displacement correlation method using linear quadrilateral elements with 12 subdivisions along the radius and along the quarter of the crack front. FEM calculations are carried out using the equivalent domain J-integral method with 36,583 tetrahedra. Note that an elastic modulus of 10,000 and a Poisson's ratio of 0.0 are assigned to the model, and a uniform, far-field tension of unity is applied.

Table 2.1: Average Mode I SIF values along the crack front calculated by the BEM and the FEM compared with the analytical solution.

Solution method	Penny-shaped	% Error
Analytical	0.357	-
BEM	0.348	2.6
FEM	0.352	1.4

The second example is a single, internal, flat, elliptical crack in an infinite body with an elastic modulus of 10,000 and a Poisson's ratio of 0.0. The orientation of the crack is the same as in Figure 2.5. An elliptical crack with 0.1 minor and 0.2 major axis dimensions is embedded in a 10 x 5 x 5 block. A uniform far-field tension of unity is applied. The analytic solution of K_I involves elliptic integrals whereas K_{II} and K_{III} are zero. Detailed discussion of the analytical solution can be found in [19]. Comparison of solutions from the BEM, and FEM and the analytical solution are given in Table 2.2. BEM calculations are done using the displacement correlation method with linear quadrilateral elements with 5 subdivisions along the axes and 12 subdivisions along the quarter of the crack front. The FEM results are computed using J-integral method with 13,464 tetrahedra.

Table 2.2: Maximum and minimum Mode I SIF values along the crack front calculated by the BEM and the FEM compared with the analytical solution.

Solution method	Max K_I	% Error	Min K_I	% Error
Analytical	0.463	-	0.327	-
BEM	0.435	5.9	0.304	7.0
FEM	0.442	4.5	0.333	1.8

2.4 Determining New Crack Front

Crack extension due to one non-proportional load cycle is computed using the approach developed in [1]. As previously mentioned, a modified Paris model was used that accounts for crack closure effects. A crack is assumed to advance when its SIF is large enough to overcome closure and is larger than the SIF of the previous load step. The new crack front is determined as follows:

1. For every point along the crack front:
   a) Calculate amount of crack growth, da^i corresponding to each load step i= 1,…15.

$$da^i = \frac{K_I^{\,i} - K_I^{\,i-1}}{\Delta K_{eff}} da$$

$$\frac{da}{dN} = C(\Delta K_{eff})^n$$

$$\Delta K_{eff} = K_I^{\max} - K_{op}$$

$$\frac{K_{op}}{K_{\max}} = A_0 + A_1 R + A_2 R^2 + A_3 R^3 \qquad \text{for } R \geq 0$$

$$A_0 = (0.825 - 0.34\alpha + 0.05\alpha^2)\left[\cos(\frac{\pi S_{\max}}{2\sigma_0})\right]^{1/\alpha}$$

$$A_1 = (0.415\alpha - 0.071\alpha^2)\frac{S_{\max}}{\sigma_0}$$

$$A_2 = 1 - A_0 - A_1 - A_3$$

$$A_3 = 2A_0 + A_1 - 1$$

   b) Calculate the angle of crack growth corresponding to each load step using maximum circumferential stress theory

$$\theta^i = 2\tan^{-1}\left[\frac{1}{4}\frac{K_I^{\,i}}{K_{II}^{\,i}} \pm \frac{1}{4}\sqrt{(\frac{K_I^{\,i}}{K_{II}^{\,i}})^2 + 8}\right]$$

   c) Calculate the final coordinates of the crack front and trajectory angles by approximating the contributions from each load step by a straight line.
   d) Determine number of cycles, N, necessary to have a reasonable amount of crack advance compared to pinion's geometry.
2. Update geometry using the new crack front points.
3. Repeat 1 and 2 for each crack growth step.

2.5 Results

Three-dimensional finite element analyses were performed for an OH-58 spiral bevel pinion for 54 crack growth steps, Figure 2.6. In the previous BEM-based analysis, only 13 growth steps were performed. One crack growth step consists of 15 static finite element analyses in order to simulate moving loads on the pinion tooth. After the 54th crack growth step the analysis was stopped because it was concluded that propagating the crack further would not provide additional insights into the simulations and results. All predictions were based on the methodology outlined in section 2.

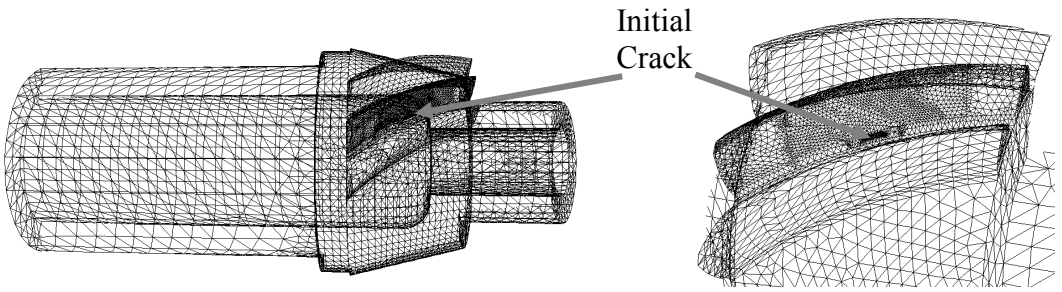

Figure 2.6: A spiral bevel pinion model with surface FE mesh (a) whole pinion (b) close-up view of pinion teeth. Note the location of the initial crack in the middle tooth.

Figures 2.7 through Figure 2.9 show Mode I, II and III stress intensity factors for the initial crack configuration for the first eleven load steps. Load steps 1-4 correspond to double tooth contact, load steps 5-11 correspond to single tooth contact and load steps 12-15 again correspond to double tooth contact. Since a crack is not assumed to advance when its SIF is smaller than the SIF of the previous load step, only the first 11 steps practically contribute to crack growth calculations. In these figures crack front position corresponds to the points near the crack front at which SIF values are evaluated. In the initial step of crack growth simulations the crack front was discretized such that there were 222 points at which SIF values were calculated. This is compared to only 61 points previously used with the BEM model [1].

Figure 2.10 shows the crack trajectory predictions by the FEM on the tooth surface and cross section of the tooth for several crack growth steps including the initial and final configurations of the crack. Figure 2.11 is a close-up view of the last step of crack growth from the toe end of the tooth.

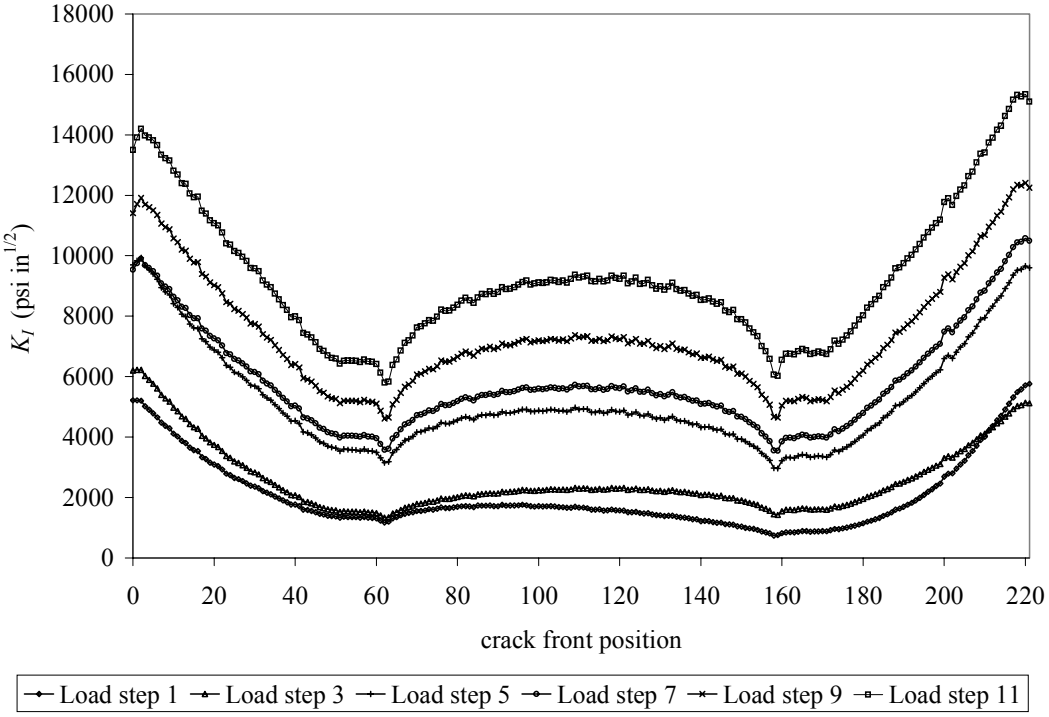

Figure 2.7: Initial Mode I SIF distribution for load steps one through eleven. Note that orientation is from heel to toe.

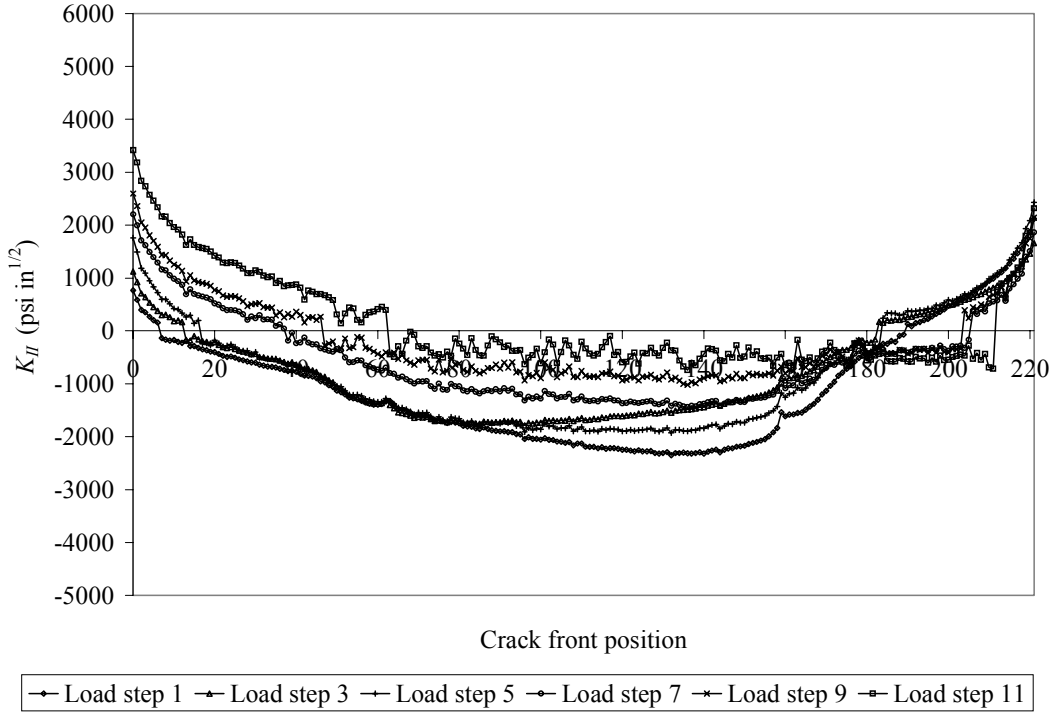

Figure 2.8: Initial Mode II SIF distribution for load steps one through eleven. Note that orientation is from heel to toe.

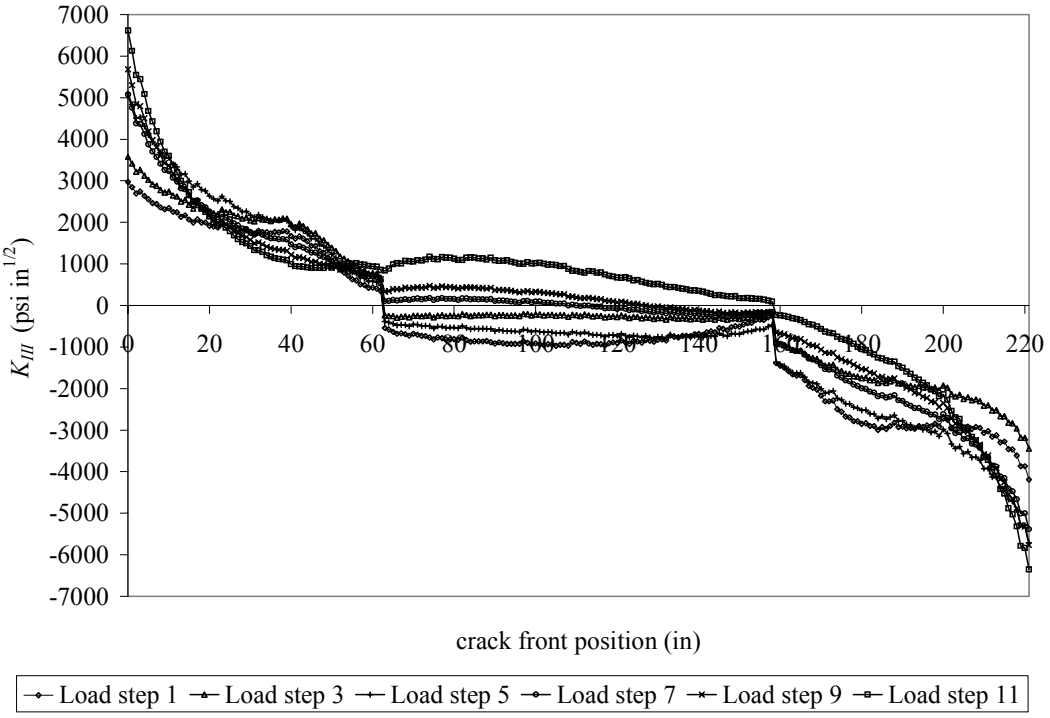

Figure 2.9: Initial Mode III SIF distribution for load steps one through eleven. Note that orientation is from heel to toe.

Initial Step: Step 0:

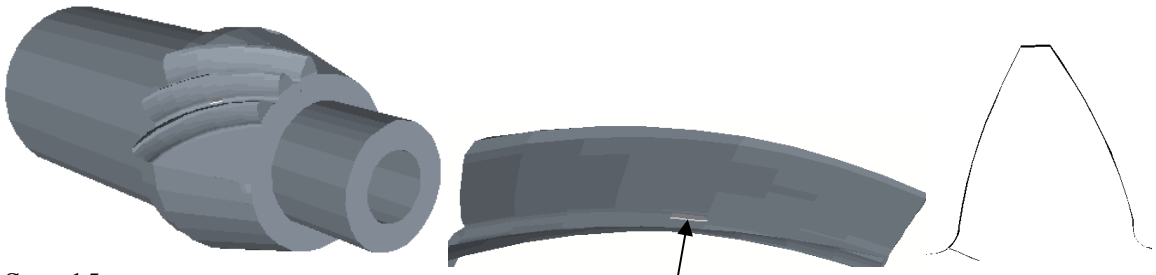

Step 15:

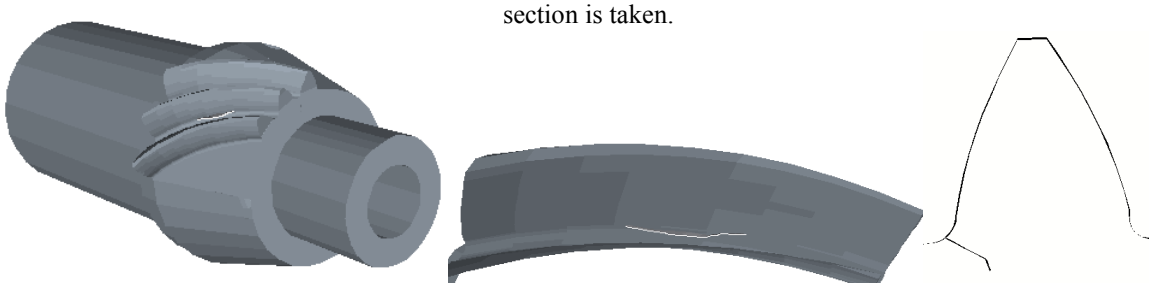

Step30:

Step 45:

Final Step: Step 54:

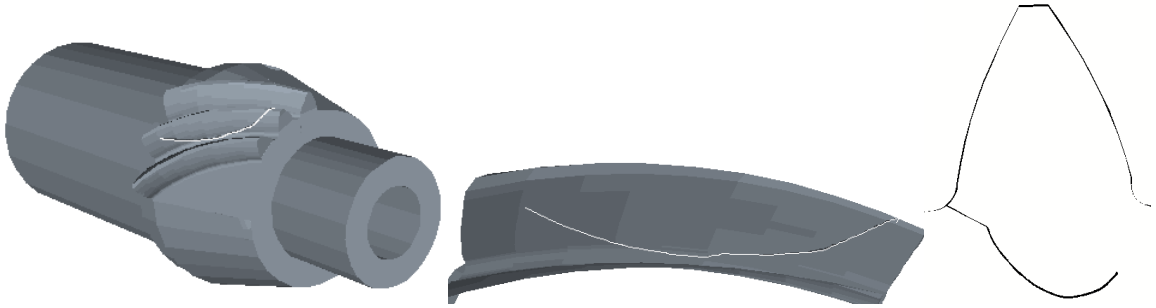

Figure 2.10: Crack trajectory predictions by FEM on tooth surface and tooth cross section.

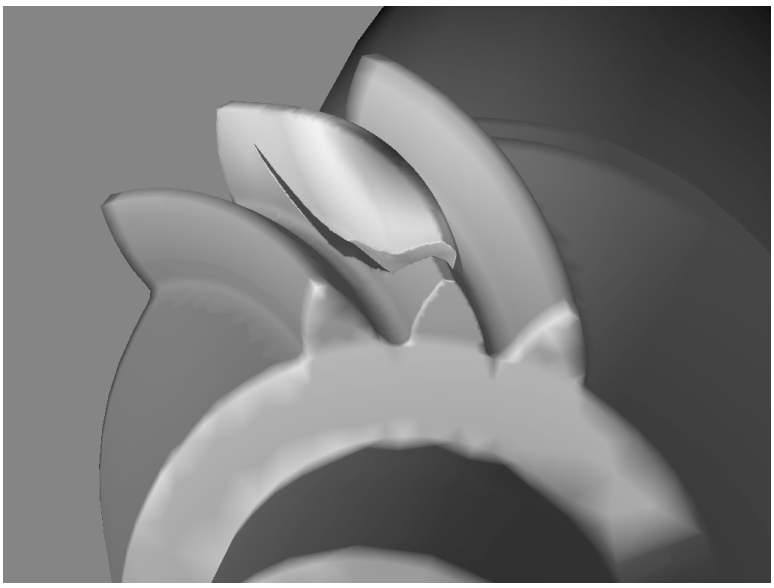

Figure 2.11: Close-up view of the crack after the last step of crack growth.

2.6 Comparison of FEM and BEM Results

This section compares FEM and BEM results in terms of accuracy and efficiency. BEM results presented in this section are from reference [1]. One of the most significant improvements in the FEM approach over the BEM simulations is the difference in the solution time of the problem. This comparison is summarized in Table 2.3.

Table 2.3: Comparison of performance between FEM and BEM simulations.

Results	FEM	BEM
Computer power	32 nodes[#] PC-cluster, 1 GHz	Single DEC-Alpha Workstation, 175 MHz
Number of unknowns (coefficient matrix)	~1-3 million (sparse, symmetric)	6700 (dense, unsymmetric)
Solution time per load cycle (1 load cycle=15 load steps)	5-15 hours (20min-1 h/load step)	~60 hours (4 models)
Typical time for one crack step	~8-18 hours[*]	~65 hours[†]

[#]Only one processor per node is used.
[*]Solution time plus 3 hours post-processing and remeshing
[†]Solution time plus 5 hours post-processing and remeshing

The performance comparison in Table 2.3 clearly shows that there is a very significant improvement in computation time with the development of a parallel FEM solver. The solution time for BEM simulations was about 65 hours for one crack growth step whereas FEM simulations took much less time for each crack growth step even though the models have many more degrees of freedom. The number of unknowns for the

FEM was about a million at the initial step and increased to more than 3 million as the crack front advanced. 3D volume meshing of one model ranged from 20 minutes for the smallest model to about an hour for the largest models.

Improvement in the computation time for each crack growth step allowed us to increase solution resolution by taking smaller crack increment steps and to simulate more steps of propagation. Figures 2.12 to 2.14 show the comparison of crack area, depth and crack front length by FEM and BEM. These plots indicate that the FEM-predicted fatigue growth rate is marginally lower when we compare the crack area and the crack front length and more cycles are required to achieve the same amount of crack growth when compared with previous BEM-based results. Figures 2.15 to 2.17 show the SIF comparisons between FEM and BEM for load steps 3, 7, and 11.

Table 2.4: Comparison of crack growth amount between FEM and BEM simulations.

Results	FEM	BEM
Number of steps	54	13
Total number of cycles	383,000	311,000
Final crack front length	1.55 in	1.42 in
Final crack area	0.319 in^2	0.186 in^2
Final crack depth	0.268 in	0.188 in

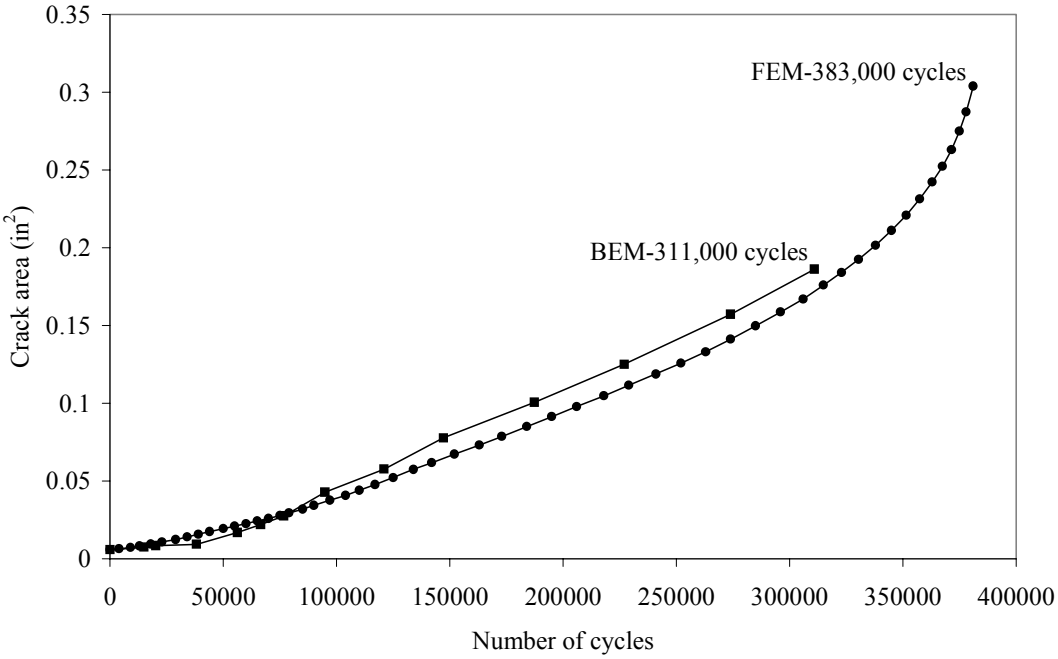

Figure 2.12: Comparison between crack area versus number of cycles predicted by BEM and FEM analyses.

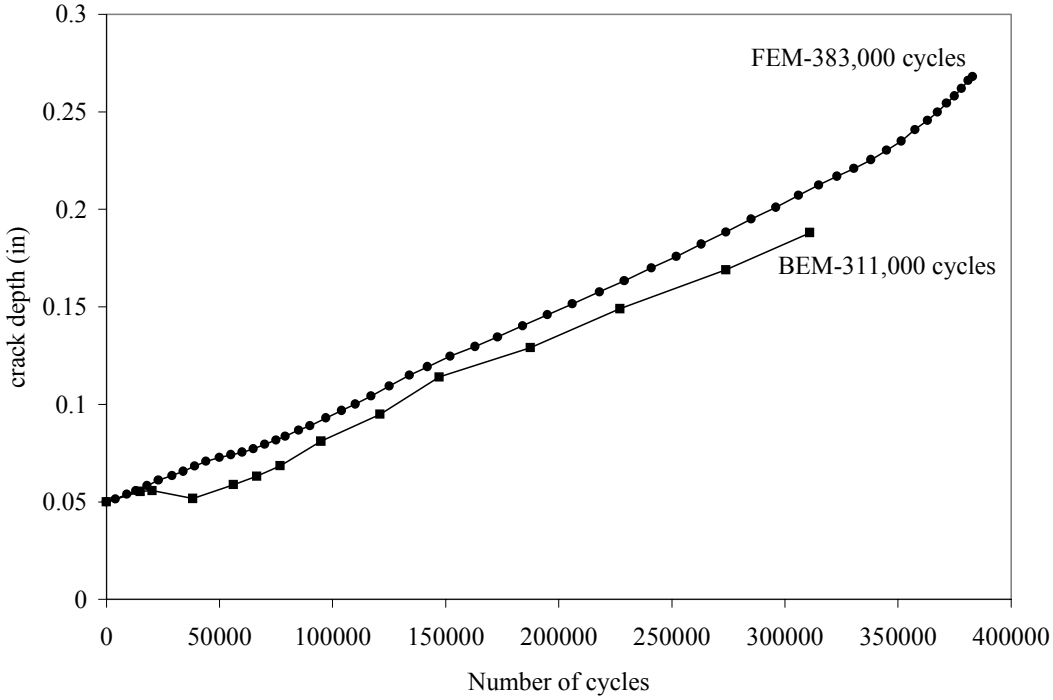

Figure 2.13: Comparison between crack depth versus number of cycles predicted by BEM and FEM analyses.

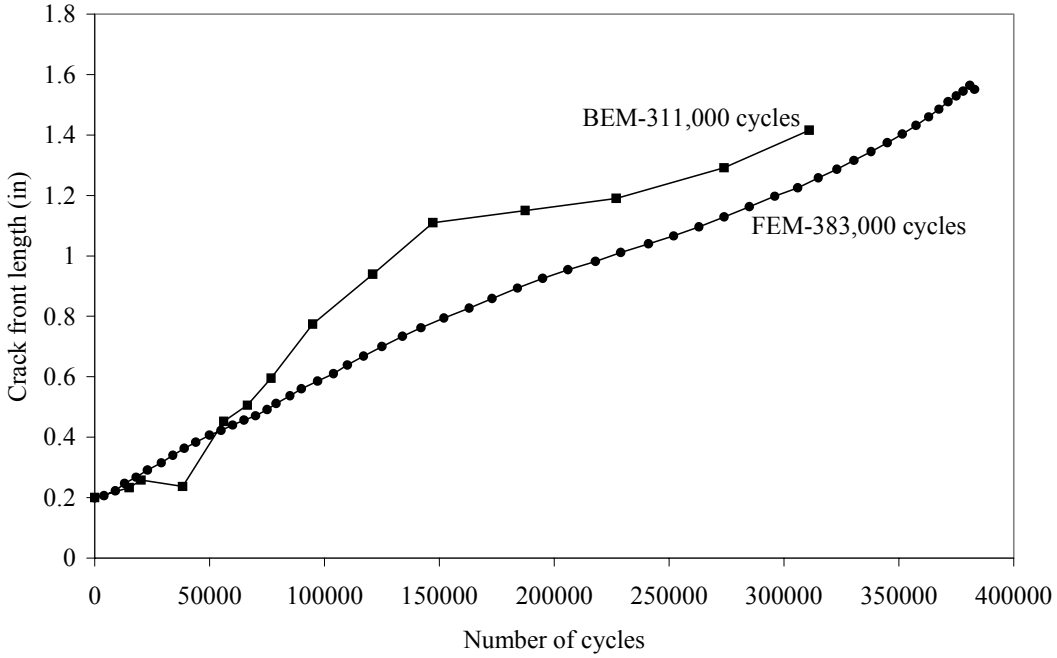

Figure 2.14: Comparison of crack front length between BEM and FEM analyses.

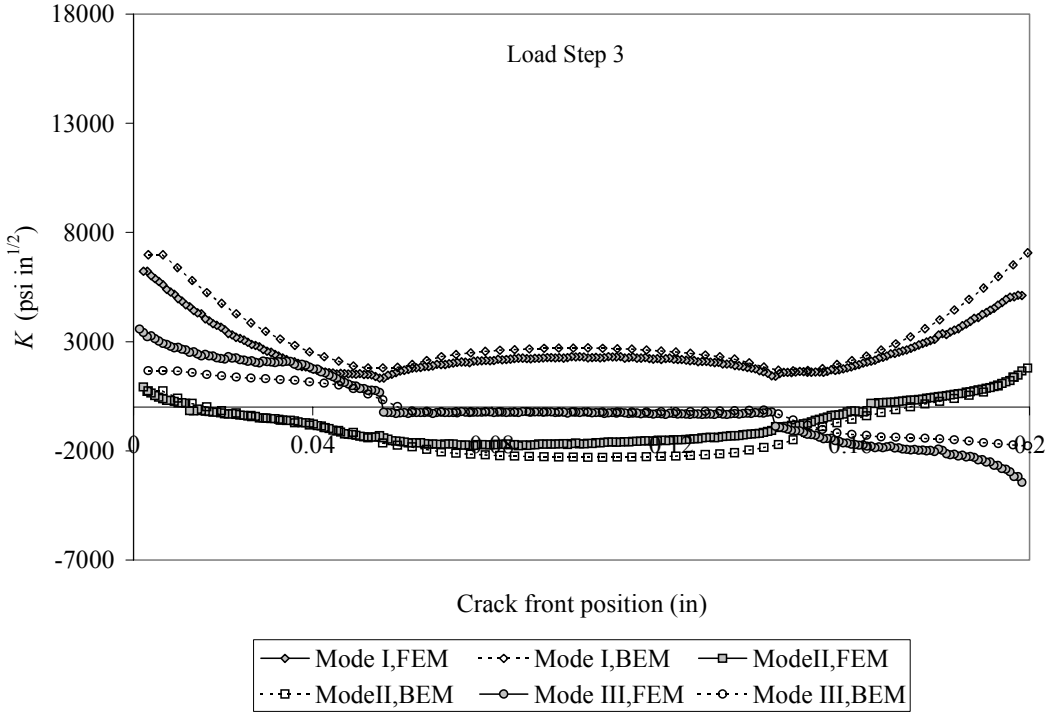

Figure 2.15: Comparison of initial Mode I, II and III SIFs computed by the FEM and the BEM for load step 3.

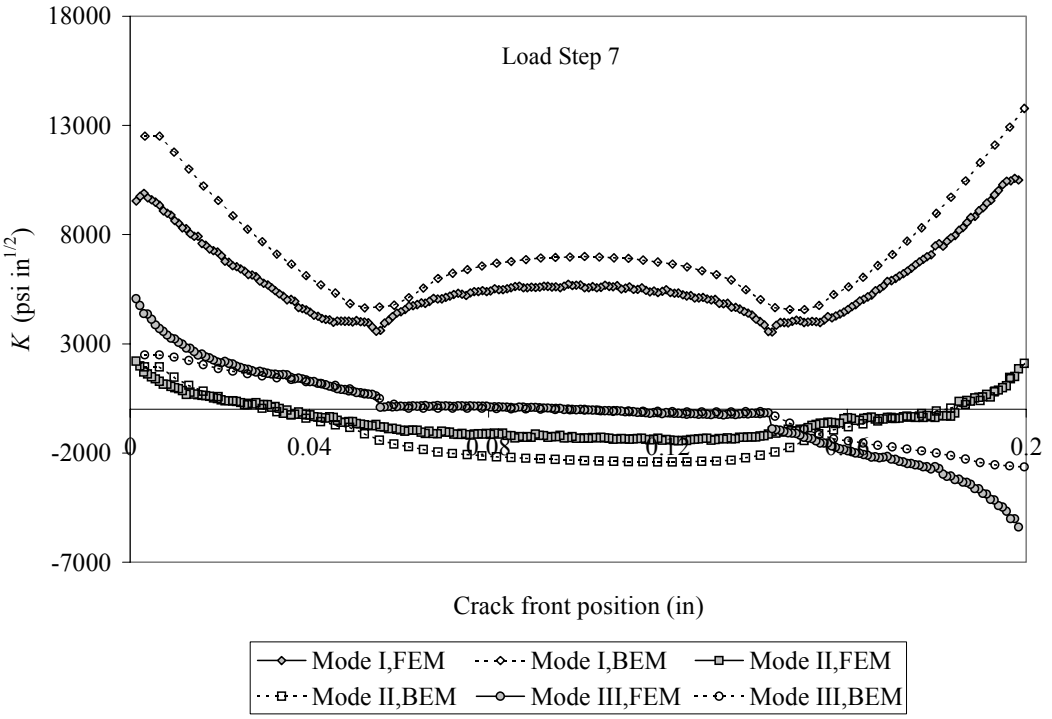

Figure 2.16: Comparison of initial Mode I, II and III SIFs computed by the FEM and the BEM for load step 7.

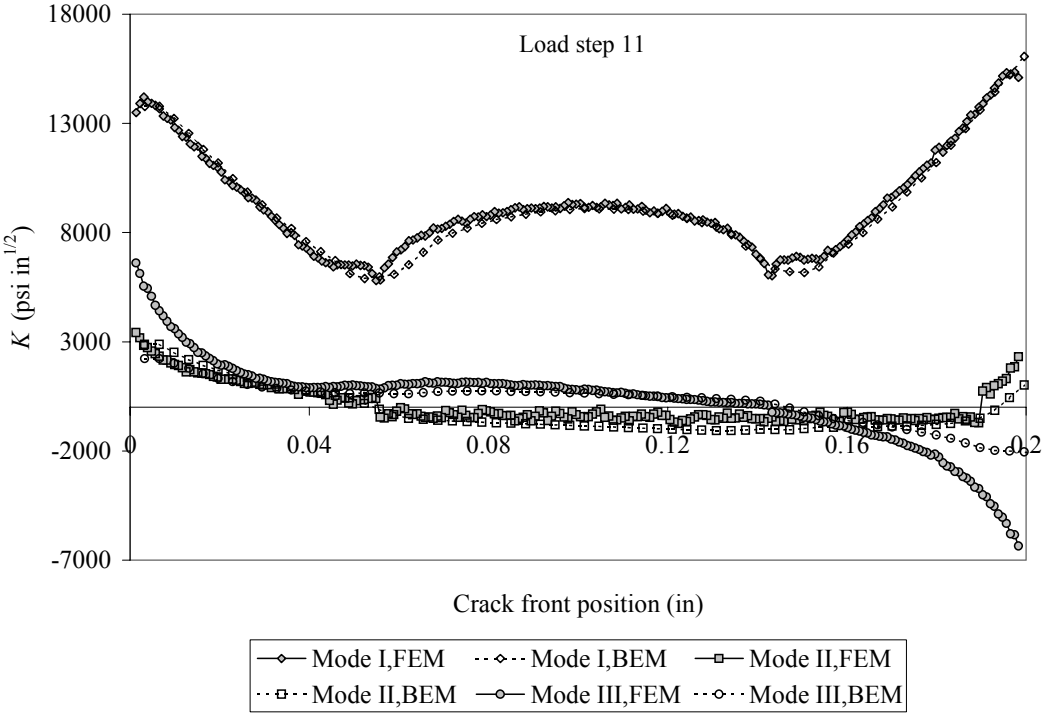

Figure 2.17: Comparison of initial Mode I, II and III SIFs computed by the FEM and the BEM for load step 11.

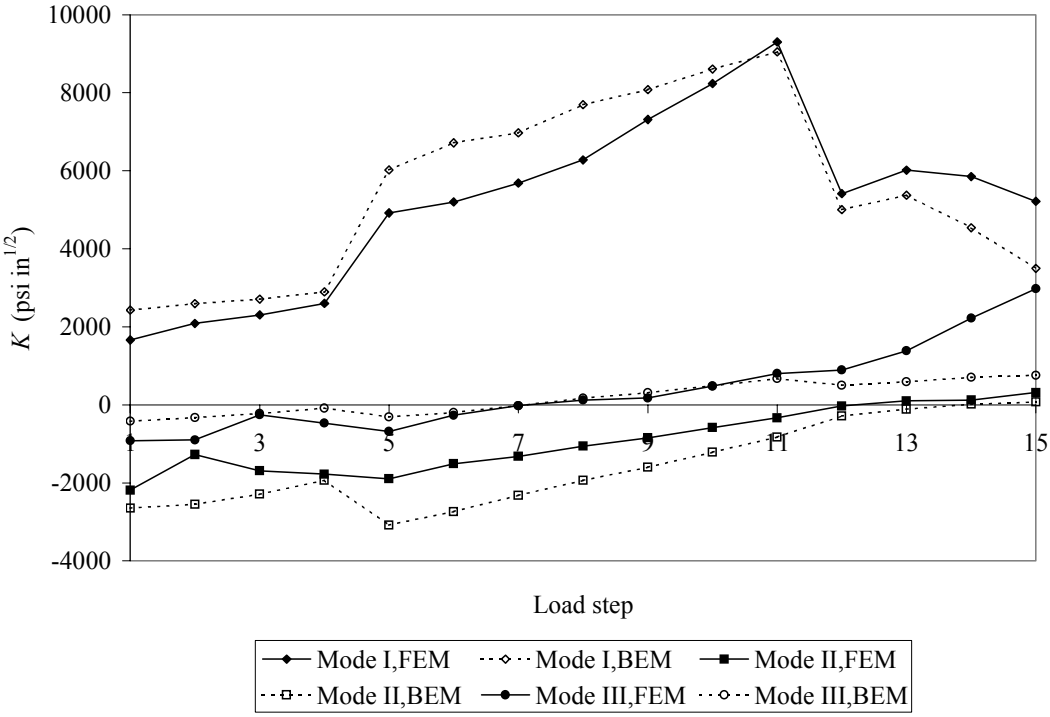

Figure 2.18: Comparison of typical SIF history computed by the FEM and the BEM for a load cycle at the midpoint of the initial crack front.

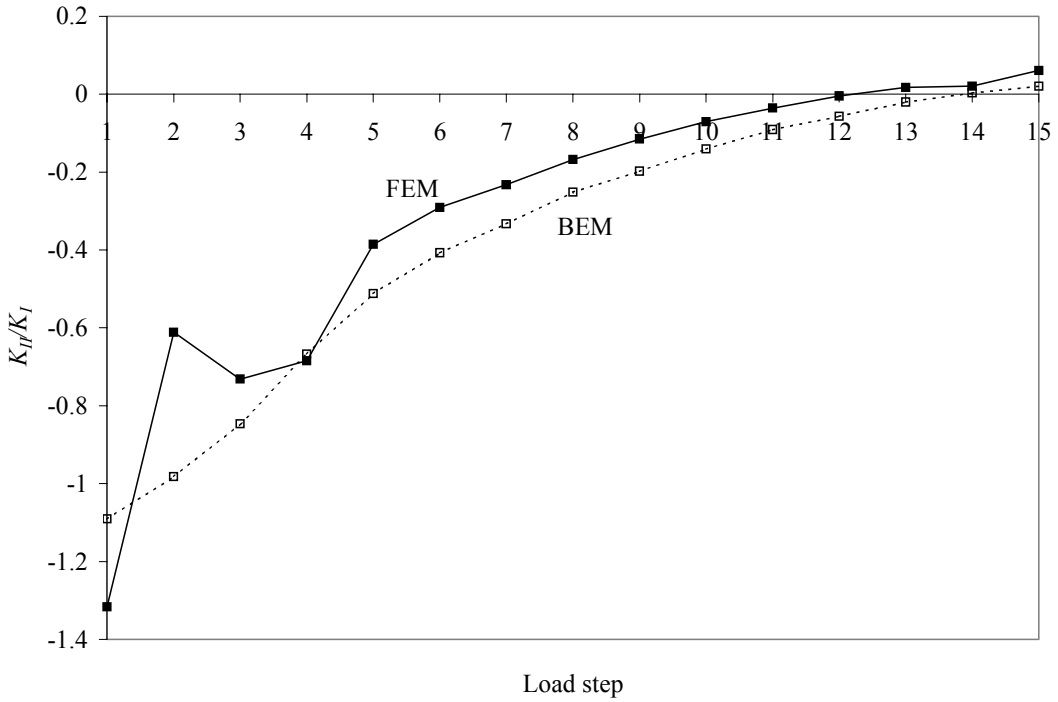

Figure 2.19: Comparison of typical non-proportional load cycle at the midpoint of the initial crack front computed by the FEM and the BEM.

Figures 2.18 and 2.19 present the comparison of SIF variation over one load cycle and non-proportional load history. In Figure 2.18, it is seen that K_I predictions are lower in the FEM analysis than the BEM analysis over most of the steps. As seen in Figure 2.19, the ratio of K_{II} to K_I over 15 load steps shows a similar trend as observed in the BEM analysis with a slight difference in values.

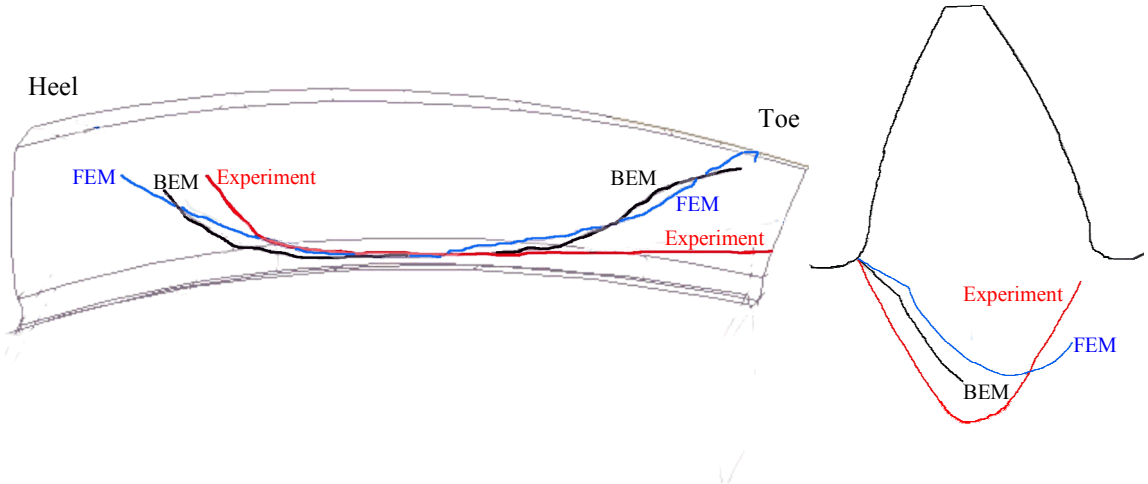

Figure 2.20: Comparison of crack trajectory predicted by the BEM, the FEM and an experiment on the tooth surface and tooth cross section at the midpoint of crack.

Crack trajectory comparisons in Figure 2.20 show that, on the tooth surface, crack trajectory predicted by FEM is similar to the BEM results. The deviation of crack path at the toe end in the BEM predictions was also observed in FEM predictions. On the heel end, FEM results exhibit a less steep propagation angle than the experimental trajectory. On the tooth cross-section it is observed that the predicted crack trajectory by FEM is less steep than BEM and experimental results. FEM results also exhibit a shallower ridge formation than the experiment. Although the FEM-predicted crack path still does not exactly represent the crack trajectory observed in experiments, it captures the global behavior of the crack propagation trajectory.

3. Three-dimensional Finite Element Contact Analysis

The meshing of a gear and pinion produces loads on the tooth surface that change in magnitude and position in time. In section 2.1 analyses assuming Hertzian contact theory were described. This assumption, however, is a simplification for a number of reasons: 1) the teeth and rims that transmit the load are flexible, 2) assumed elliptical contact area on the tooth surface may not be accurate since the curvatures of the teeth surfaces in contact are not constant over the contact zone, 3) the center of contact, where the maximum contact stress occurs, may differ from the theoretical contact point, and 4) most importantly for the current investigation, the tooth flexibility changes as the crack propagates in a tooth. The change in flexibility due to cracks may shift the contact area, and change the magnitude of the contact loading.

In this section a series of three-dimensional finite element analyses that model the contact conditions between the gear and pinion explicitly are described. The purpose of this study is to assess what influence the details of the load transfer through the contact conditions have on the computed stress intensity factors, and through them the predicted crack trajectory.

Three-dimensional finite element contact analyses in spiral bevel gears have been undertaken by several researchers to study the stresses induced at the root and on the surface of the tooth. Earlier work by Bibel *et al.* [20] utilized gap elements to simulate the contact boundary conditions and to evaluate the stresses on the tooth surface. Further study on this subject eliminated the need of using gap elements through the use of contact capabilities of commercial finite element programs. Preliminary results showing the moving contact patches over the tooth surface are reported in Bibel and Handschuh [21]. These analyses also incorporate automatic meshing of the gear and pinion via the addition of user subroutines to a commercial finite element program. The same authors performed additional analyses in order to compare experimentally measured tooth bending stresses of spiral bevel gears to FEM results [22]. Other studies on the contact analysis of spiral bevel gears, including the development of a methodology combining a surface integral and a finite element solution, are described by Vijakaar [23]. Numerical examples carried out using this approach show the change in the contact area as a result of the misalignment of the gears.

3.1 Approach

The goal of the present study is to perform contact analyses incorporating cracks to determine the effect of changing tooth flexibility on the magnitude and location of the contact load and therefore on the stress intensity factors. A commercial finite element program, ABAQUS [24], was used to perform the contact analysis in conjunction with the software developed by the CFG to calculate fracture-related parameters. A general outline of the approach is as follows:

1. Create initial geometry model of spiral bevel pinion and gear with OSM using the geometry information provided by NASA Glenn Research Center.
2. Specify boundary conditions, material properties, and contact surfaces in FRANC3D.
3. Create a surface mesh composed of triangular elements in FRANC3D.
4. Create a 3D FE mesh of the model composed of tetrahedra using the J-mesh program.
5. Transform the FRANC3D model into an ABAQUS input file.
6. Perform contact analysis in ABAQUS and determine the location and magnitude of the contact loads.
7. Calculate SIFs using the results of FEM contact analysis and also using the results from analysis with Hertzian contact loads. Compare these values and investigate their effects on the crack trajectory predictions.

Geometries of a one-tooth sector of the spiral bevel pinion and gear were created separately in OSM using the information provided by NASA. This information regarding the geometric positions of points defining the gear set was determined analytically using the method developed by Litvin *et al.* [3]. The one-tooth gear and pinion models were created in a common coordinate system with the same axis of rotation (z-axis). Additional teeth of the gear and pinion were created by copying and rotating the original tooth by an angle equal to 360º divided by number of gear teeth. The resulting models were further rotated to orient them in the proper meshing position. At the meshing orientation there was no interference between the gear and pinion teeth.

The contact analysis was performed using the contact pair approach in ABAQUS. Contact pairs, named as master and slave surfaces, define surfaces which can potentially come into contact. If one of the contact surfaces is stiffer or has a coarser mesh, that should be selected as the master surface. In this formulation contact direction is always normal to the master surface. In ABAQUS, contact can occur in the form of small-sliding or finite-sliding. Analyses performed in this work used the finite-sliding formulation where surfaces are allowed to undergo finite separation and sliding. This formulation defines the master surface as composed of element faces. Continuity of the surface normals was attained by smoothing the transitions between the elements. Contact surface tractions were calculated assuming that the surfaces are perfectly hard, which means there will be no penetration of surfaces into one another. Contact tractions were defined by the local basis system formed by the normal to the master surface.

The analyses used both FRANC3D and ABAQUS. FRANC3D was used to generate the complicated geometry of the gear, to specify the analysis attributes, and to define the

crack. Also, it was used as a post-processor to calculate the SIFs. ABAQUS was utilized for finite element contact analysis of the model. In order to perform contact analysis on models with cracks, features that complement FRANC3D and ABAQUS were needed. In this respect FRANC3D was extended to include a capability of specifying the master and slave contact surfaces and to include a translator to convert the information regarding the geometry, mesh, boundary conditions, material properties and contact surfaces to an ABAQUS input file. Also, equivalent domain J-integral implementation was added to FRANC3D to obtain more accurate SIF values.

Contact analyses involve nonlinear geometric analysis. The gear/pinion model is meshed with linear tetrahedra. Volume meshing is done using J-mesh as before. The mesh is finer on the contacting tooth surfaces of both gear and pinion compared to the rest of the model. In performing the analyses, it was assumed that there was no friction between the contacting surfaces.

3.2 Analysis

Finite element contact analysis of a spiral bevel gear and pinion was performed on a four-tooth model composed of two pinion teeth and two gear teeth. This model is shown in Figure 3.1 and is adapted from [22]. Only four teeth of the gear and pinion were explicitly modeled since this is the minimum number of teeth that is needed to simulate double tooth contact. We chose to model only a small portion of the gear and pinion to decrease the computation time and effort. This model was adequate to simulate the contact conditions and also demonstrate how the stress intensity factors change with increasing crack length.

The model was designed such that load applied at a known distance from the axis of rotation transmits the required amount of torque. The gear model was extended to include a solid, "wedge shaped" part. This portion was a modeling artifact added so that the gear could be allowed to rotate freely about its axis of rotation and come into contact with the pinion as a result of the applied torque. As seen in Figure 3.1a, the pinion teeth were fixed with zero displacements in x,y,z directions on the rim surfaces. Displacement components of the gear were fixed in x,y,z directions along the line of axis of rotation. Gear rim surfaces were only constrained in the z direction; x and y degrees of freedom of the gear were not fixed in order to allow for free rotation in that plane. Dimensions of the gear sector were chosen such that the bending effects caused by the application of load is minimized. Early studies showed that when smaller portions of the gear were modeled contact loads changed with the change in the location of the applied load due to the excessive deformation occurring in the gear hub.

Full design torque for the pinion was 3099 in-lb. In order to obtain the torque that is transferred by the gear this value was multiplied by the gear ratio, giving 11580 in-lb. A point load was applied at a distance 3.58 in. from the gear axis of rotation to produce this amount of torque. The location of the applied load is shown in Figure 3.1a.

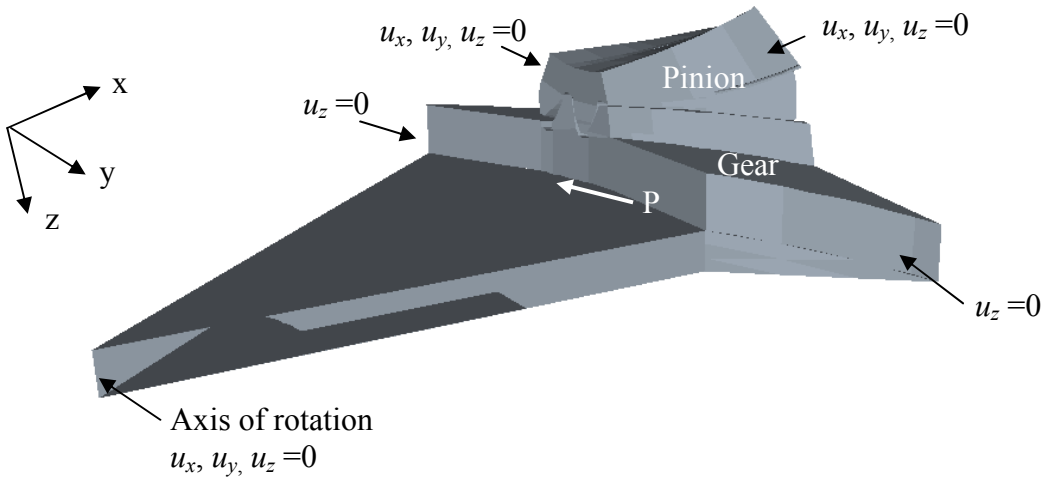

(a)

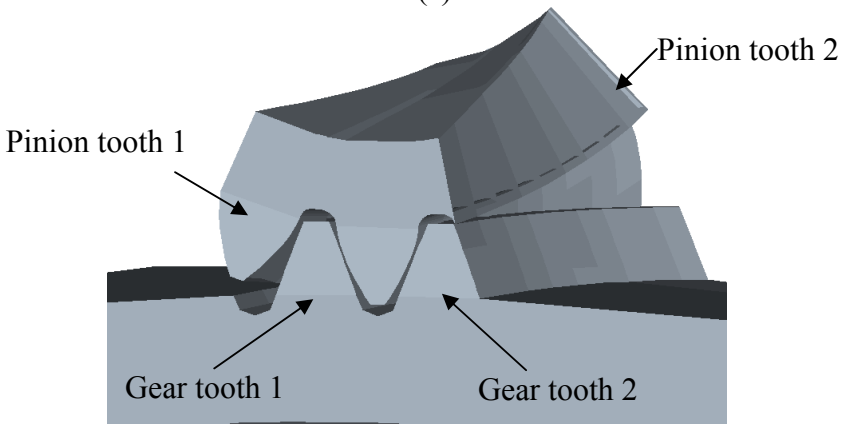

(b)

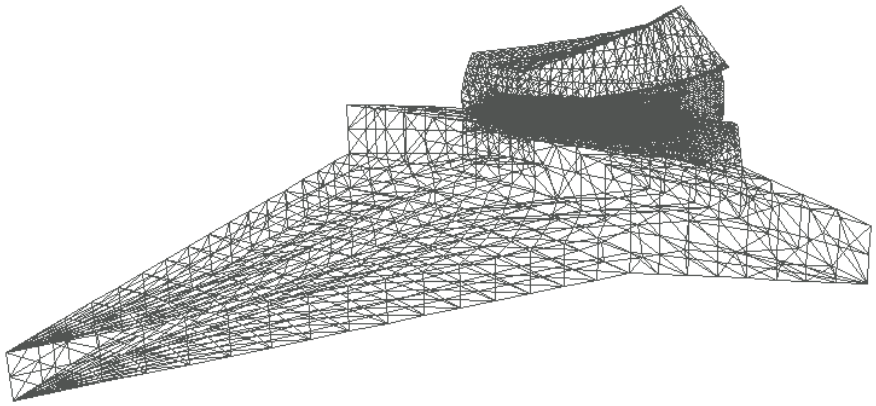

(c)

Figure 3.1: Contact model of spiral bevel gear set. (a) whole model (b) close up view of gear and pinion teeth in mesh (c) FE mesh of the model. Note that two teeth of pinion and gear are explicitly modeled. Note also the refined mesh on the pinion and gear teeth surfaces where contact is expected to occur.

The original configuration of the gear and pinion corresponds to a double tooth contact load transfer. In order to obtain a single tooth contact configuration the gear set was rotated equivalent to a 12º pinion rotation. During the analyses, first a very low displacement was applied to the gear in order to ensure contact between gear and pinion and to fix the model in space. Then the load was increased to its full design value.

In order to obtain reasonable contact loads, an adequately refined mesh was very important. Since the gear has a doubly curved geometry, a fine discretization was needed to model the curved edges. In our studies, we observed that coarse meshes lead to inaccurate contact stresses and stress concentrations. To this end, we discretized the surfaces where contact is expected to occur fine enough to obtain reasonable results without excessive computational cost.

3.3 Results

Contact analyses were carried out on four models which have: no crack, an initial crack, and two crack sizes, crack #1 and crack #2. Crack #1 is within the fillet region of the pinion tooth. Crack #2 is a larger crack extending to the surface of the tooth. These four geometries were analyzed for double tooth contact and single tooth contact configurations that correspond to 0° and 12° pinion rotation, respectively.

The number of nodes and elements for the analyzed models ranged between 12,000-16,000 and 52,000-70,000, respectively. Solution time of a finite element contact analysis is about 30 minutes on a 1 GHz Intel Pentium III machine.

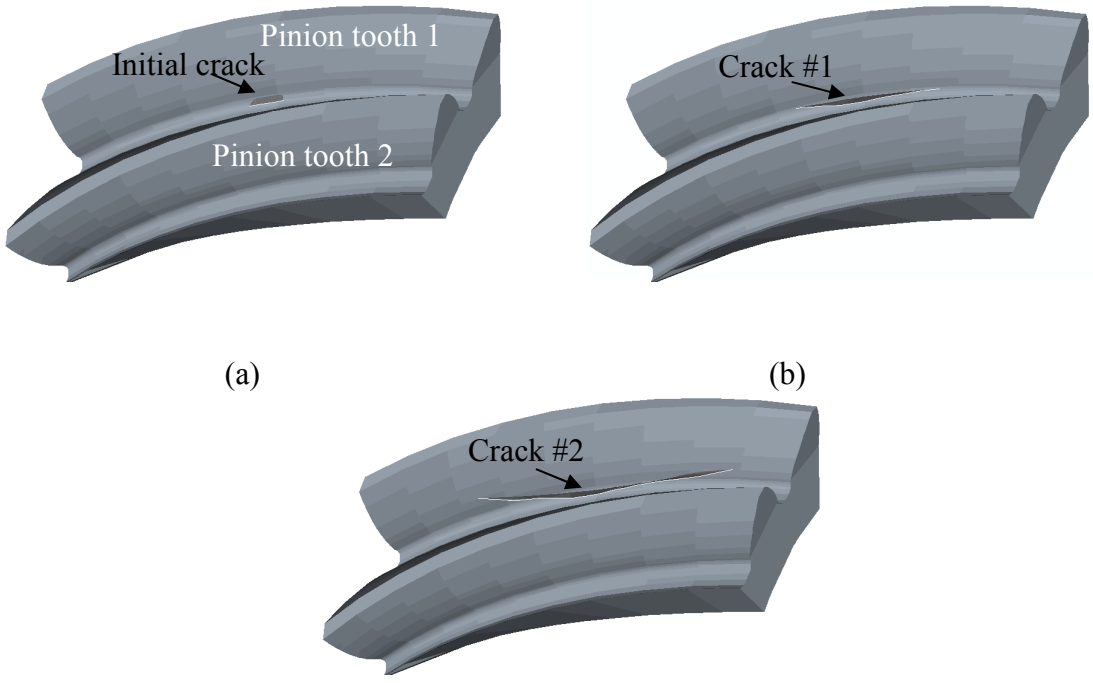

Figure 3.2: Pinion teeth with a) initial crack b) crack #1 c) crack #2. Note that in all the models, crack is in tooth 1.

3.3.1 Comparison of contact load and area calculated by Hertz theory and three-dimensional FEM contact analysis

Results of contact analyses and how they compare to the Hertz theory are summarized in Table 3.1. Total contact load calculated by finite element analysis compared well with the total load predicted by Hertz theory. However, distribution of this total contact load between two adjacent teeth shows some discrepancies. There is nearly a 10% difference in the values between contact analysis and Hertz theory predictions on each tooth.

We were unable to attain single tooth contact conditions using this model. At all rotations, there is always at least a very little portion carried by the adjacent tooth. This might be due to the inaccuracies introduced by the geometric model of the gears. The closest case to single tooth loading was obtained when a 12º pinion rotation was introduced to the model. This case was assumed to correspond to load step 11 during which the highest contact load occurs.

Contact loads calculated by finite element analyses decrease on tooth 1, where the crack is located, and increase on tooth 2 as the crack grows. These results indicate that as the crack becomes larger, the flexibility of the pinion tooth is enhanced, therefore the contact loads taken up by the two adjacent teeth are redistributed. A larger portion of the total contact load has to be carried by the uncracked neighboring tooth. This trend is in agreement with the expected behavior.

Table 3.1: Comparison of contact loads and areas between FEM contact simulations and Hertzian stress calculations for two contact configurations with different crack lengths. Note that in the first configuration the Hertz contact load given below corresponds to load step 3 for tooth 1 and load step 13 for tooth 2, and in the second configuration it corresponds to load step 11.

Model	**Contact Load (lb)**		**Contact Area (in^2)**	
	Tooth #1	**Tooth #2**	**Tooth #1**	**Tooth #2**
Configuration # 1 (*Rotation 0º*)				
No crack	1800	1399	0.0129	0.0126
Initial crack	1794	1404	0.0129	0.0126
Crack #1	1792	1406	0.0123	0.0126
Crack #2	1743	1457	0.0177	0.0126
Hertz Solution	1584	1602	0.0114	0.0146
Configuration # 2 (*Rotation 12º*)				
No crack	2899	318	0.0193	0.0018
Initial crack	2885	322	0.0193	0.0018
Crack #1	2881	326	0.0193	0.0018
Crack #2	2860	348	0.0252	0.0018
Hertz Solution	3196	-	0.0216	-

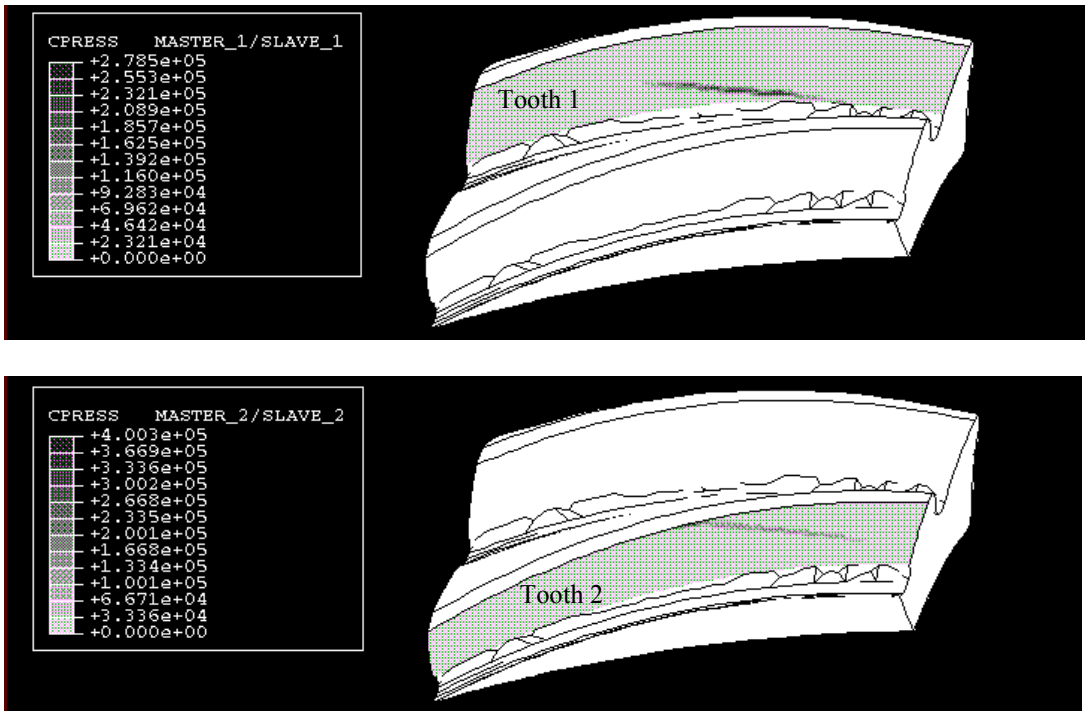
CPRESS MASTER_1/SLAVE_1
+2.785e+05
+2.553e+05
+2.321e+05
+2.089e+05
+1.857e+05
+1.625e+05
+1.392e+05
+1.160e+05
+9.283e+04
+6.962e+04
+4.642e+04
+2.321e+04
+0.000e+00
Tooth 1
CPRESS MASTER_2/SLAVE_2
+4.003e+05
+3.669e+05
+3.336e+05
+3.002e+05
+2.668e+05
+2.335e+05
+2.001e+05
+1.668e+05
+1.334e+05
+1.001e+05
+6.671e+04
+3.336e+04
+0.000e+00
Tooth 2

(a)

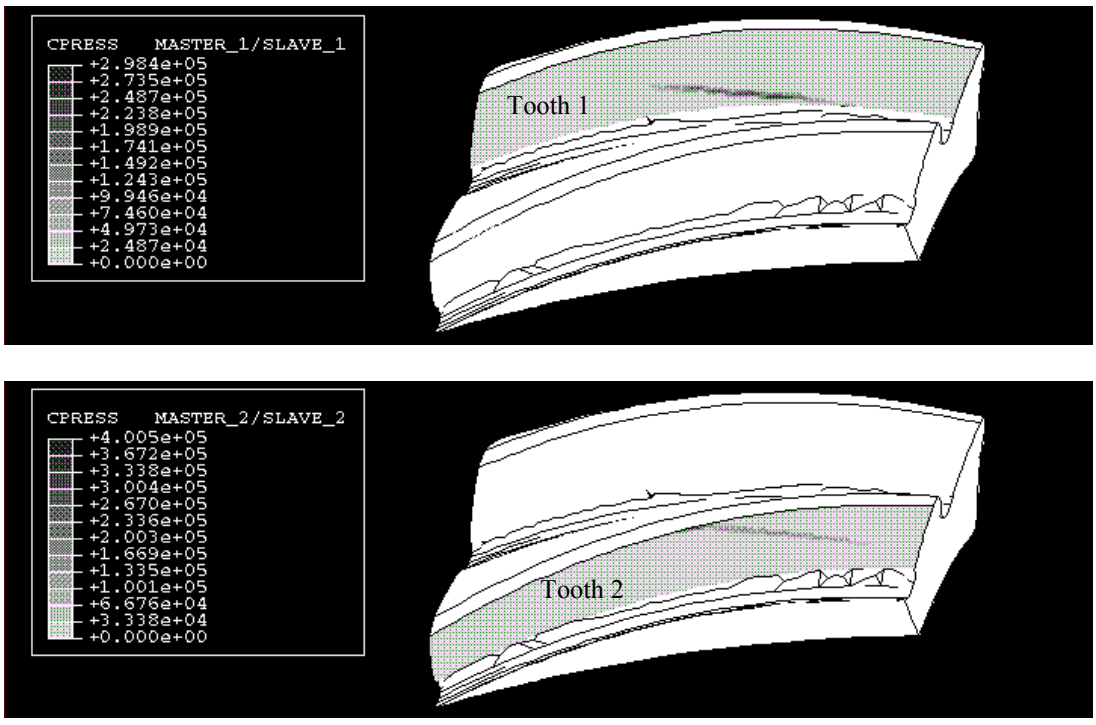
CPRESS MASTER_1/SLAVE_1
+2.984e+05
+2.735e+05
+2.487e+05
+2.238e+05
+1.989e+05
+1.741e+05
+1.492e+05
+1.243e+05
+9.946e+04
+7.460e+04
+4.973e+04
+2.487e+04
+0.000e+00
Tooth 1
CPRESS MASTER_2/SLAVE_2
+4.005e+05
+3.672e+05
+3.338e+05
+3.004e+05
+2.670e+05
+2.336e+05
+2.003e+05
+1.669e+05
+1.335e+05
+1.001e+05
+6.676e+04
+3.338e+04
+0.000e+00
Tooth 2

(b)

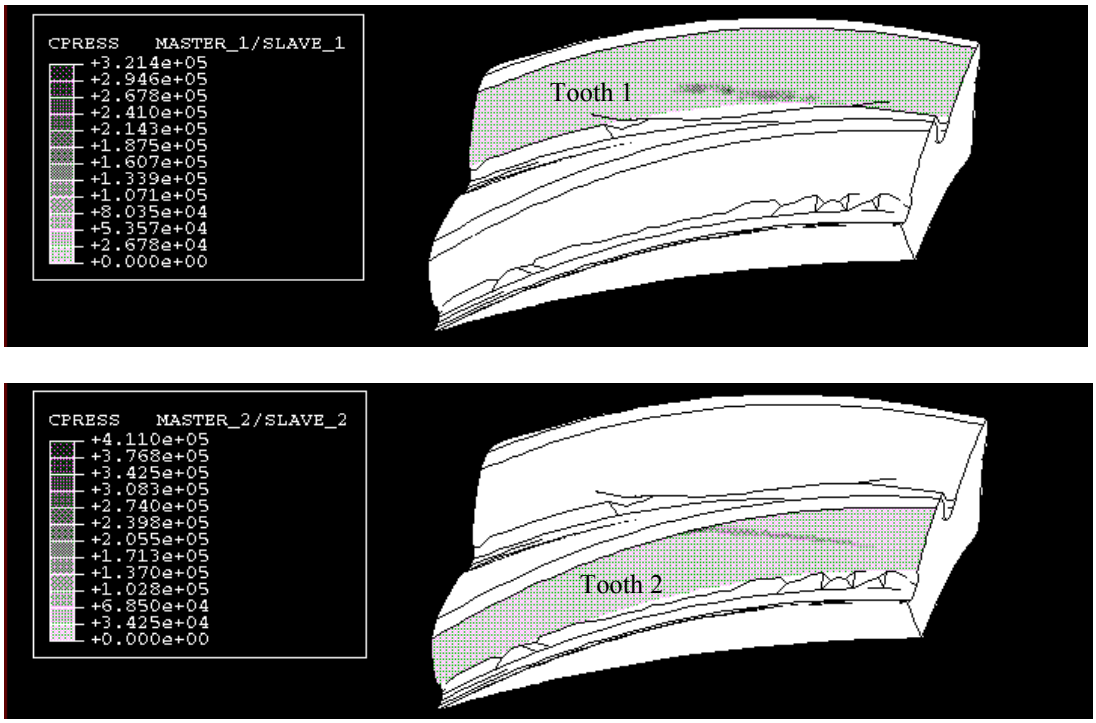

(c)

Figure 3.3: Contact pressures in on pinion tooth surface for a double tooth contact configuration with (a) initial crack (b) crack #1 (c) crack #2. Note that the values on the contour bars are in psi.

For earlier steps of the crack growth, when the crack is still in the fillet of the pinion tooth, as in crack #1, there is no significant change in the contact load and area on the tooth as seen in Table 3.1. However, when the crack extends into the tooth surface, as in crack #2, its effect on the flexibility of the tooth is more pronounced. This results in a more significant decrease in the contact load on tooth 1.

There is no significant difference in the centroid of contact loads calculated by finite element contact analysis for different crack lengths. However, locations of contact loads determined by these analyses were shifted towards the toe compared to the Hertz theory predictions.

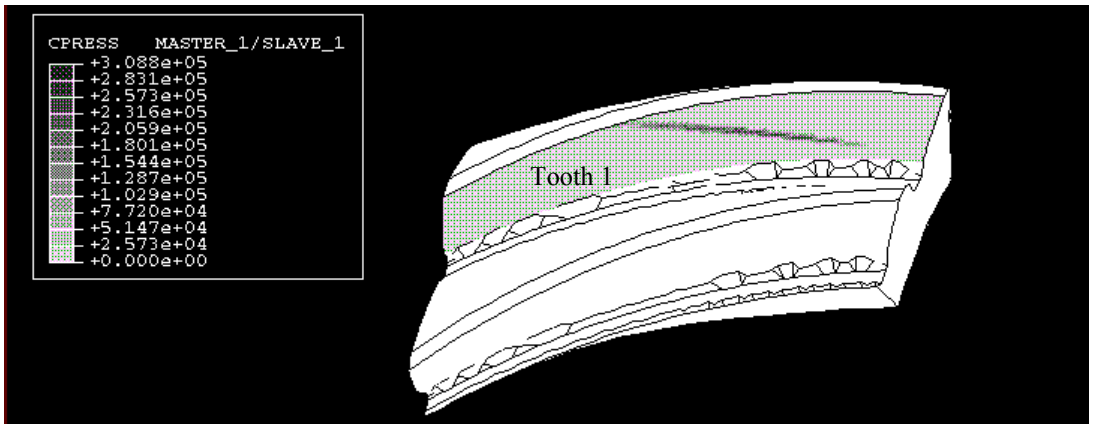

(a)

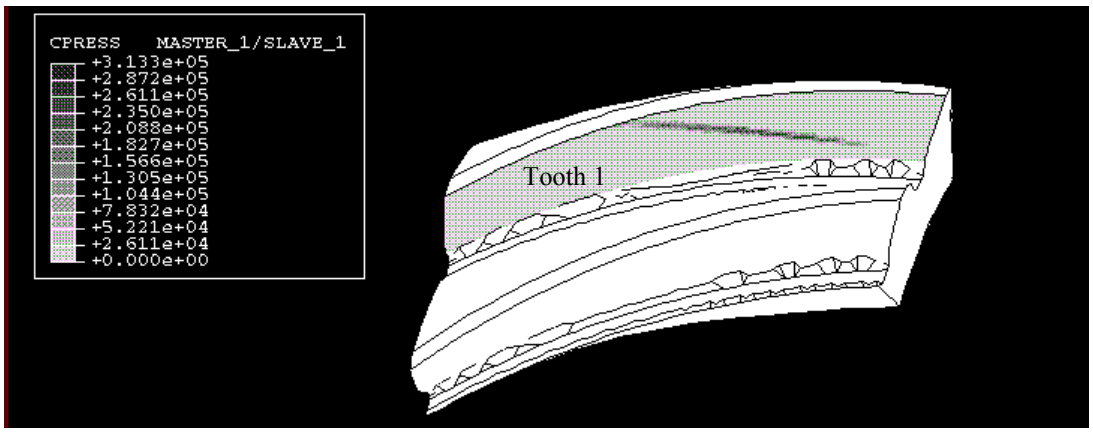

(b)

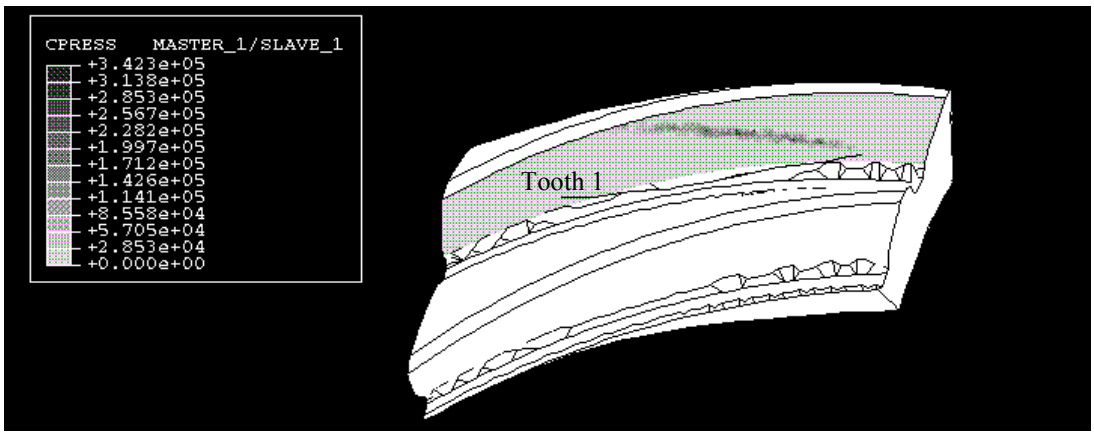

(c)

Figure 3.4: Contact pressures on pinion tooth surface for an almost single tooth contact configuration with (a) initial crack (b) crack #1 (c) crack #2. Note that the values on the contour bars are in psi.

Contact areas shown in Figures 3.3 and 3.4 are almost elliptical, showing the same trend as the Hertz contact predictions. Also, the distribution of the contact loads is close to an ellipsoid shape predicted by Hertzian contact. Maximum contact loads calculated by contact analysis were higher than the predictions by the Hertz theory.

Results of contact analyses are very sensitive to the mesh size of the contacting surfaces. If a coarse mesh is used, computed contact pressure is not continuous on the surface since only certain nodes are in contact. In order to overcome this issue, the mesh on tooth surfaces was refined several times until a continuous contact pressure distribution was obtained. The slightly wavy pattern observed in the contact areas in Figures 3.3 and 3.4 are an artifact of the mesh size, shape and orientation. Meshes on the gear and pinion tooth surfaces are built such that there is compatibility of the mesh nodes between these two contact surfaces. This is important since the contact is calculated based on the interaction of mesh nodes between contacting surfaces. If the nodes of one of the surfaces fall between the two nodes defining an edge of the other surface, then the contact load is taken up by either of the nodes that might lead to different contact patterns. The discontinuous contact load pattern observed on crack #2 (Figure 3.3c and 3.4c) for both configurations might be due to the surface mesh of the tooth. At this crack step, the crack was extended to the surface of the pinion tooth. This distorted the regularity of the mesh on the pinion surface. Since the compatibility of the meshes on both surfaces is very important for the contact analysis, the loss of this compatibility might lead to the formation of the contact areas as seen in the above figures. However, this issue does not bear a high significance for the calculation of the SIFs. For the accuracy of the SIF values, the dominating variable is the total contact load transferred rather than the exact distribution.

Figures 3.5 and 3.6 show the comparison of location of contact loads by Hertzian analysis and FE contact analysis for both single-tooth and double-tooth contact at initial crack. Gray squares in the figures define the extreme points of the Hertzian contact ellipses. Black points are the mesh nodes where contact occurs in the FE contact analysis. The location of contact loads is almost the same at crack #1 and crack #2.

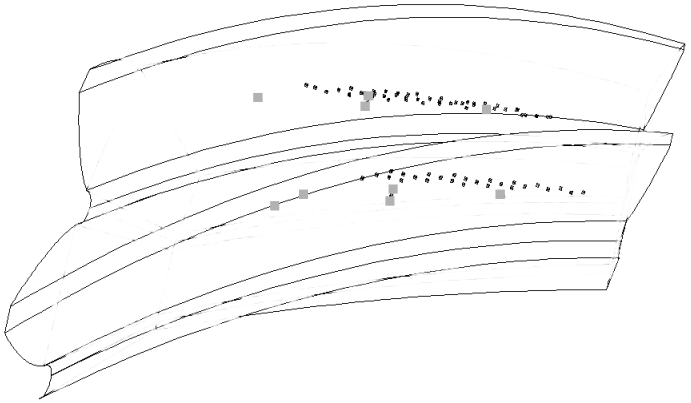

Figure 3.5: Comparison of location of contact loads by Hertzian analysis and FE contact analysis for double-tooth contact at initial crack. Hertzian loads on tooth 1 and tooth 2 correspond to load step 3 and load step 13, respectively.

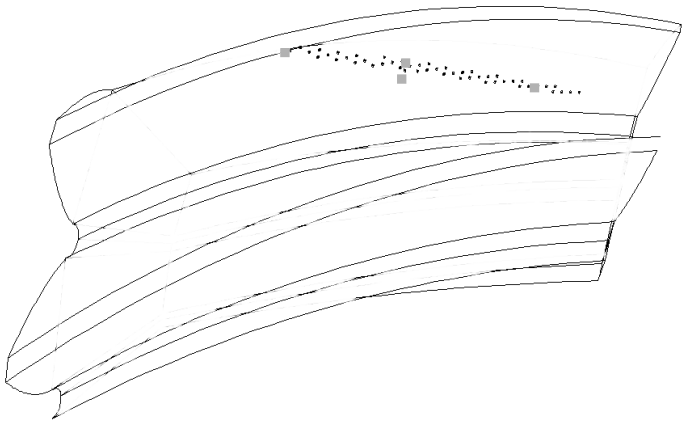

Figure 3.6: Comparison of location of contact loads by Hertzian analysis and FE contact analysis for double-tooth contact at initial crack. Hertzian load on tooth 1 corresponds to load step11.

3.3.2 Comparison of SIFs extracted from three-dimensional FEM contact analysis and finite element analysis with Hertz contact loads

Change in contact loads due to cracking is expected to have an influence on the stress intensity factors and therefore on the crack trajectory. In order to investigate this issue, SIFs were calculated using the results of three-dimensional finite element contact analysis and finite element analysis using Hertzian contact loads. The latter set of analyses were carried out using a two-tooth pinion model where the Hertzian contact loads, corresponding load step 3 and load step 11 of the fifteen discretized moving load steps described in section 2.1, were applied to the model.

SIFs were first calculated by the displacement correlation technique for both cases; however, contact analysis results did not compare well with the Hertzian contact load results. A 30 % difference in SIFs was observed between the two set of analysis. We used linear elements for contact calculations, which is required for this type of analysis, and extracted SIFs from these results by the displacement correlation technique. This approach is not accurate enough with the linear elements.

The equivalent domain J-integral method is known to give more accurate results, and this method was implemented in FRANC3D. However, SIFs obtained by linear elements were still somewhat less accurate than the quadratic elements used for the finite element analysis with Hertz contact loads. Improved results with the linear elements were obtained as the size of the radius determining the domain of the J-integral calculations increased.

Comparisons between Hertz contact loads and contact loads calculated by three-dimensional finite element analysis were given in the previous section. In this section, we present the effects of the difference in contact loads calculated by two different methods on the SIFs. Figures 3.7 through 3.12 compare mode I, II and III SIFs extracted from the results of the analyses with Hertz contact conditions and three-dimensional finite element contact analyses.

SIF values were calculated for the models mentioned in the previous section, namely, a pinion with an initial crack, and with cracks corresponding to crack #1 and

crack #2. Two loading conditions were investigated, one corresponding to double tooth contact and the other corresponding to single tooth contact, assumed to represent load step 3 and load step 11, respectively.

The difference between SIFs calculated by three-dimensional finite element contact analyses and analyses using Hertz contact loads increased as the crack length increased due to the enhanced flexibility of the tooth. The change in tooth flexibility as the crack grew, resulted in lower contact loads and therefore lower SIFs.

For the gear/pinion model with an initial crack under double-tooth contact, the difference was not expected to be that significant since the initial crack was very small and did not introduce significant additional flexibility to the tooth. This behavior is shown in Figure 3.7. At crack #1, as shown in Figure 3.8, the change in the SIFs became more pronounced. An even more amplified effect of the change in tooth flexibility was observed for crack #2, as plotted in Figure 3.9.

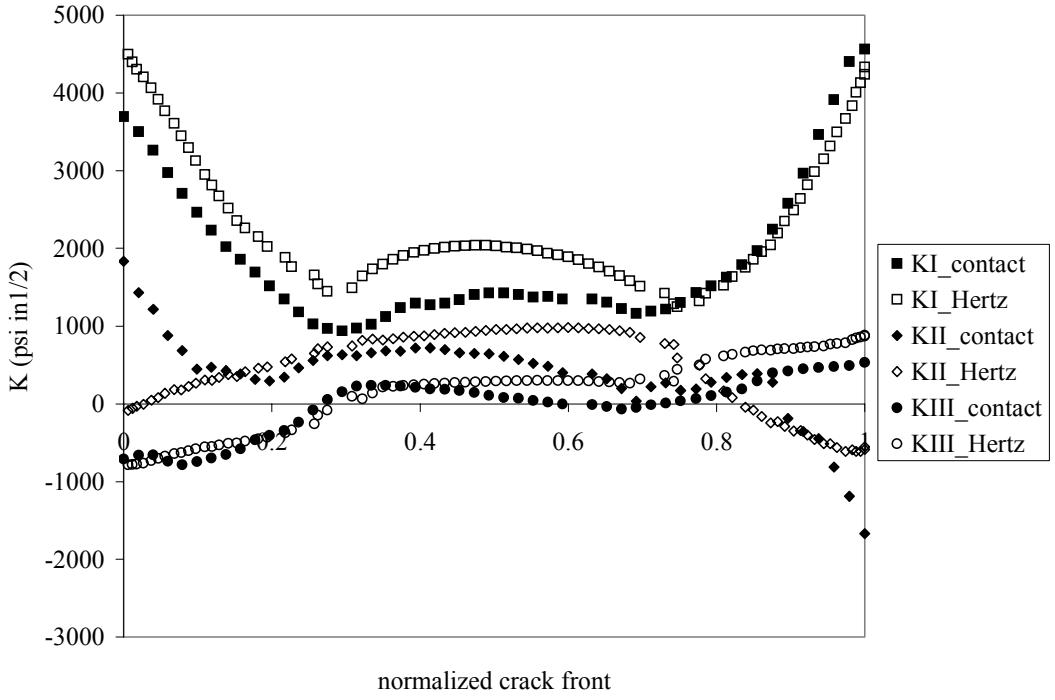

Figure 3.7: Comparison of mode I, II and III SIFs calculated by three-dimensional finite element contact analysis and finite element analysis with Hertzian contact analysis for a pinion with initial crack and at a double tooth contact configuration.

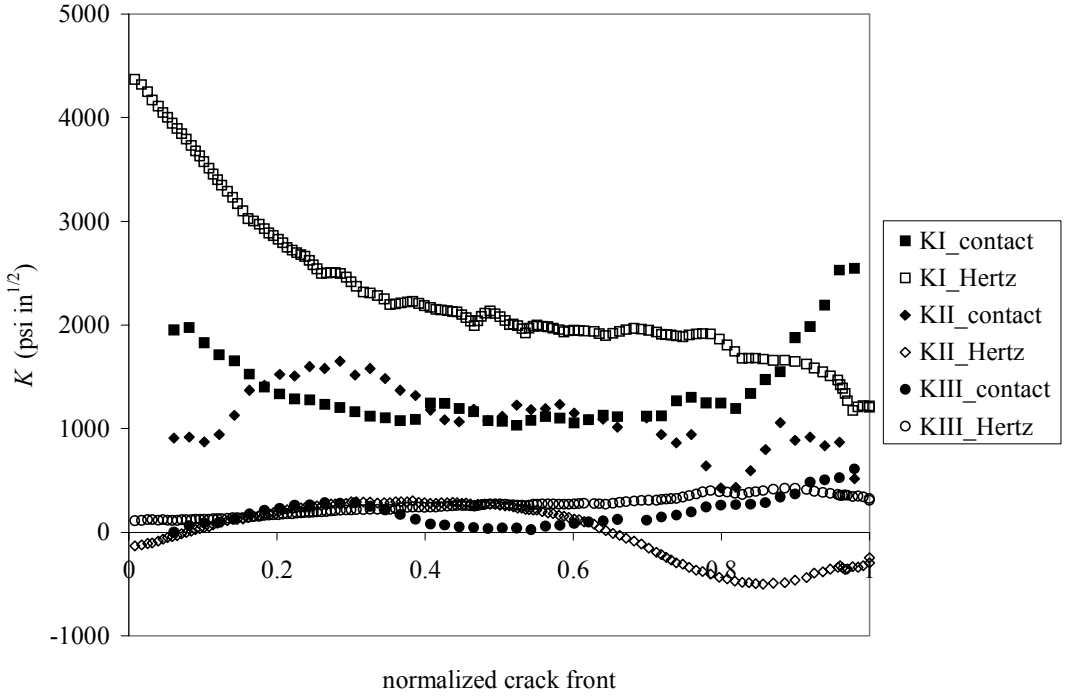

Figure 3.8: Comparison of mode I, II and III SIFs calculated by three-dimensional finite element contact analysis and finite element analysis with Hertzian contact analysis for a pinion with crack #1 and at a double tooth contact configuration.

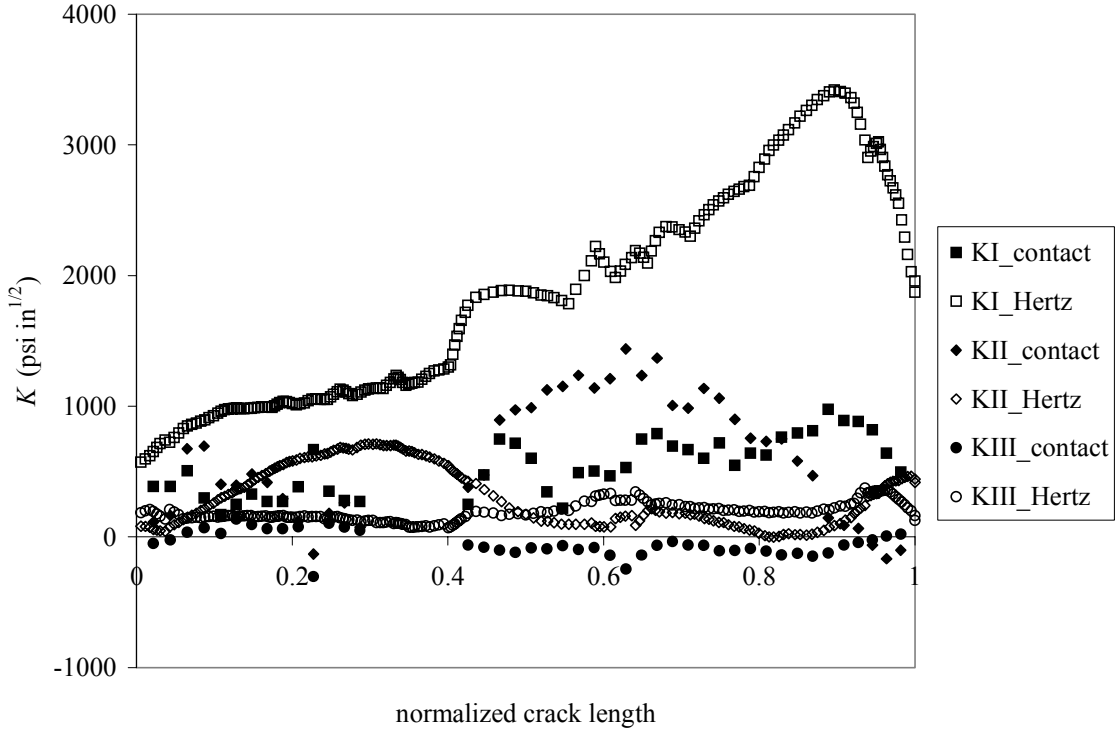

Figure 3.9: Comparison of mode I, II and III SIFs calculated by three-dimensional finite element contact analysis and finite element analysis with Hertz contact loads for a pinion with crack #2 and at a double tooth contact configuration.

The analyses were repeated for an almost single tooth contact case on all three of the crack configurations. The same trends were observed as in the double tooth contact as seen in Figures 3.10 through 3.12. However, the difference between the contact analyses and analyses with Hertz contact loads were higher for this case. This might be due to the fact that the total load applied to the tooth was less than the total load applied in analysis with Hertzian contact. As described in section 3.3.1, and shown in Table 3.1, there was at least a very little portion carried by the adjacent tooth decreasing the amount of total load carried by the cracked tooth.

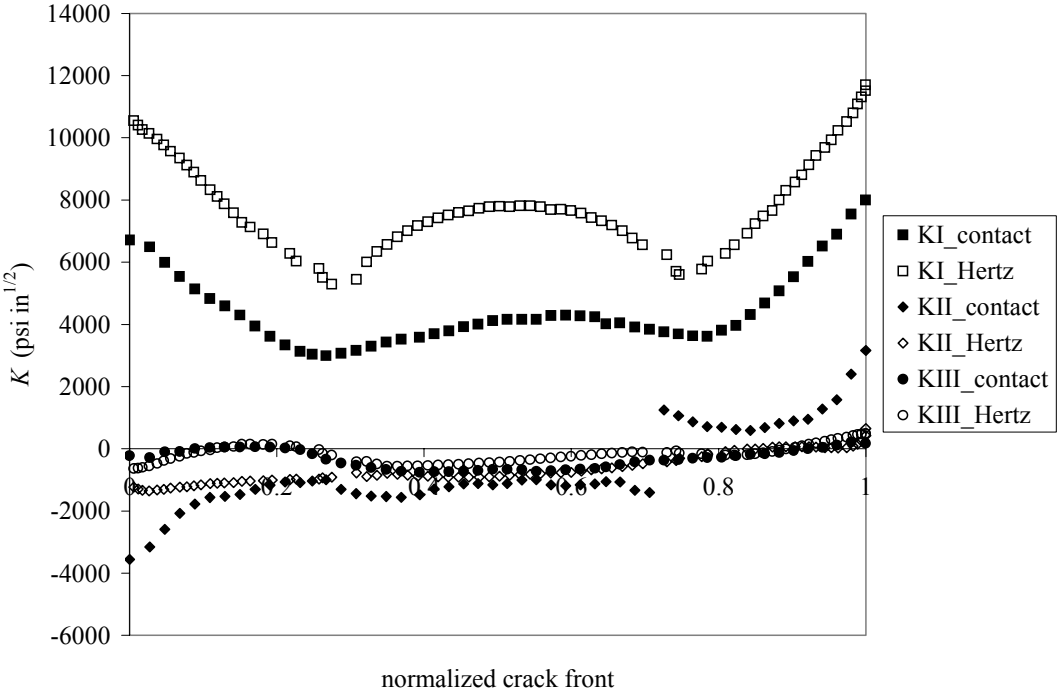

Figure 3.10: Comparison of mode I, II and III SIFs calculated by three-dimensional finite element contact analysis and finite element analysis with Hertzian contact loads for a pinion with initial crack and at a single tooth contact configuration.

Figures 3.13 through 3.15 show the variation of the ratio of K_{II} to K_I along the crack front for both double-tooth and single-tooth contact. These graphs are plotted using the results obtained by FE contact analysis for all three models with initial crack, crack #1 and crack #2.

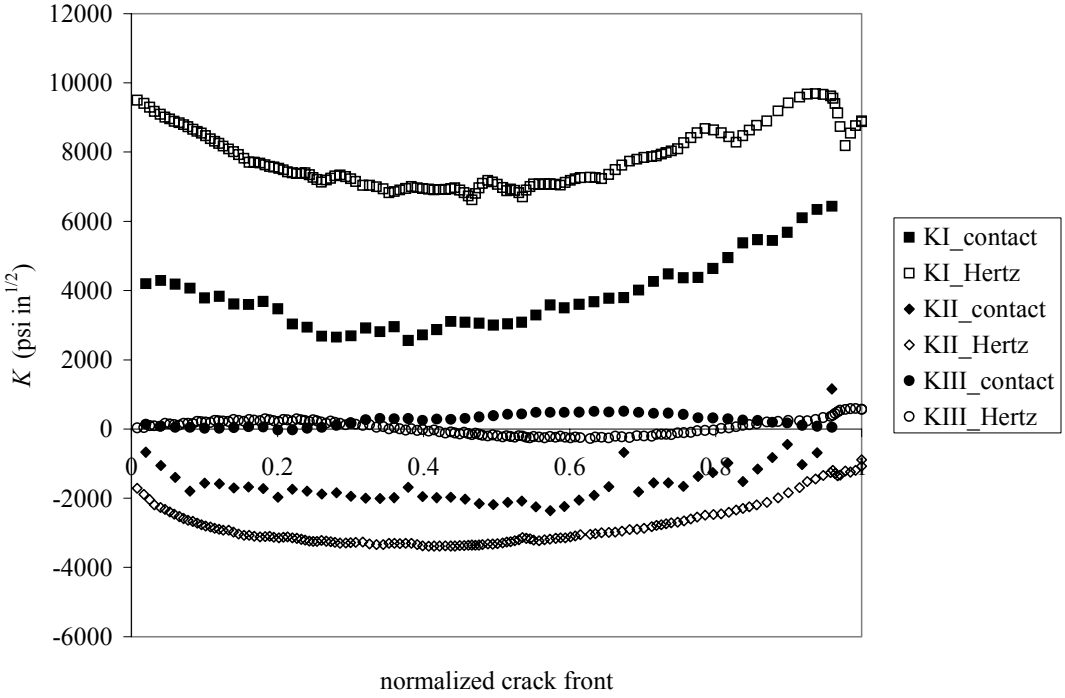

Figure 3.11: Comparison of mode I, II and III SIFs calculated by three-dimensional finite element contact analysis and finite element analysis with Hertzian contact loads for a pinion with crack #1 and at a single tooth contact configuration.

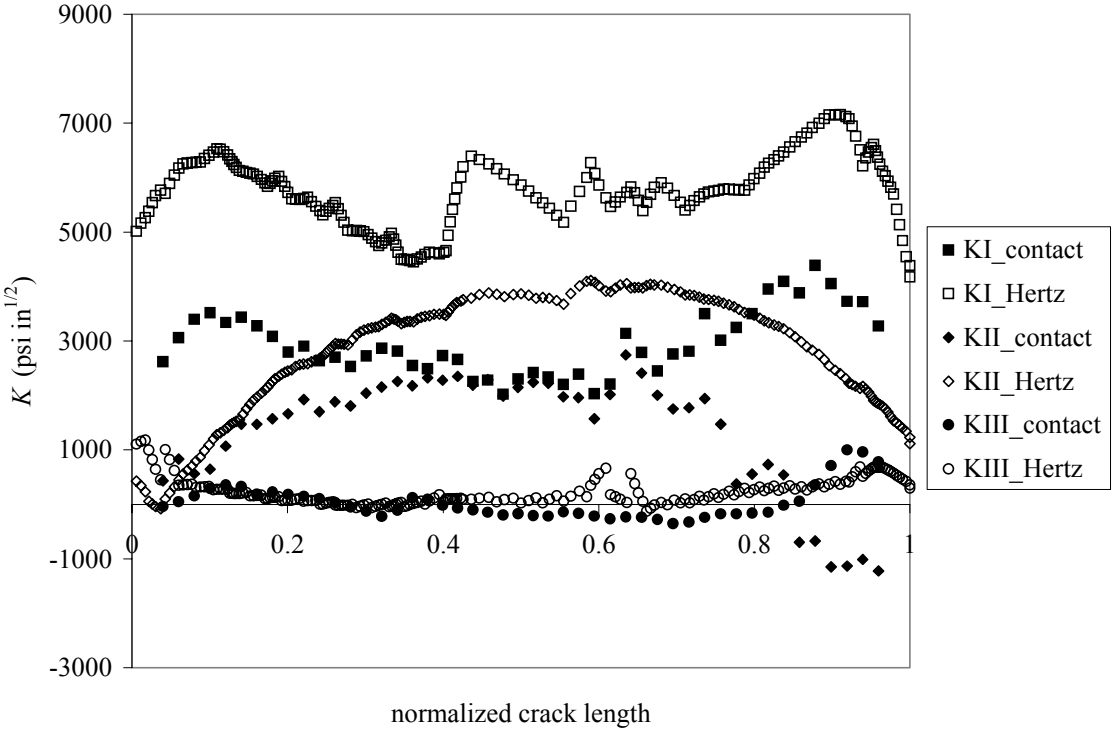

Figure 3.12: Comparison of mode I, II and III SIFs calculated by three-dimensional finite element contact analysis and finite element analysis with Hertzian contact loads for a pinion with crack #2 and at a single tooth contact configuration.

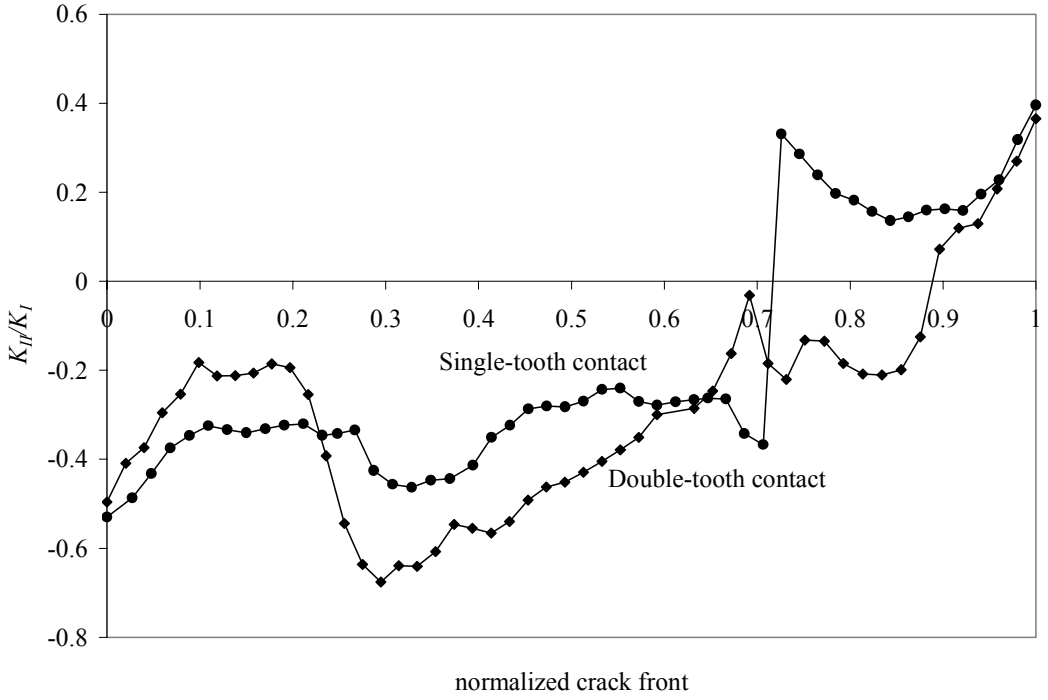

Figure 3.13: Ratio of K_{II} to K_I along the crack front for double-tooth and single-tooth contact at initial crack.

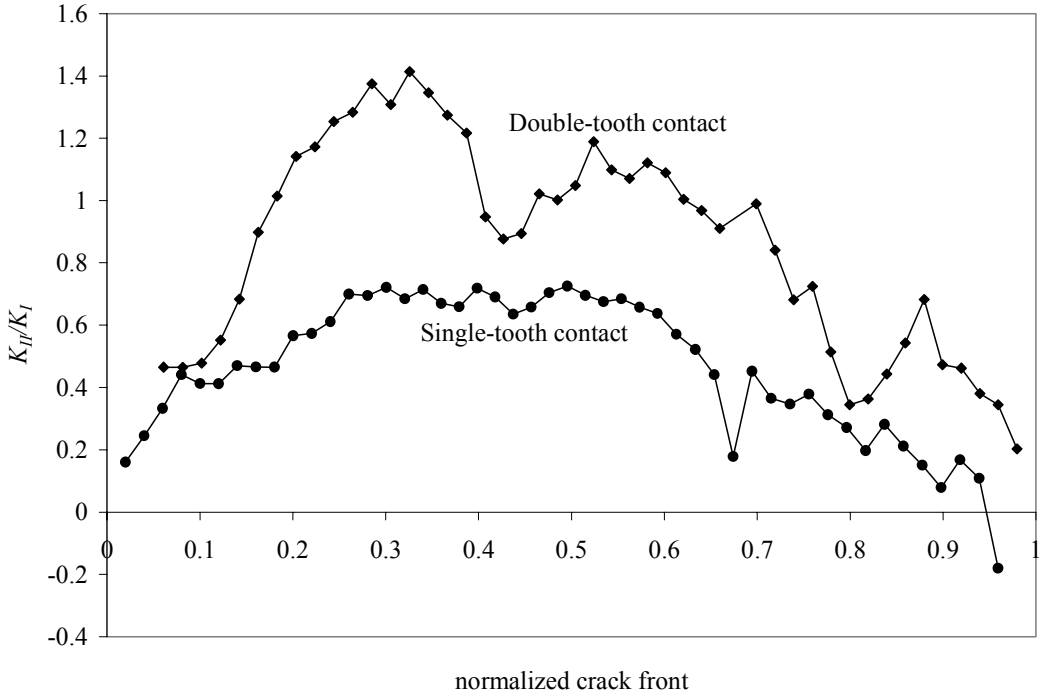

Figure 3.14: Ratio of K_{II} to K_I along the crack front for double-tooth and single-tooth contact at crack #1.

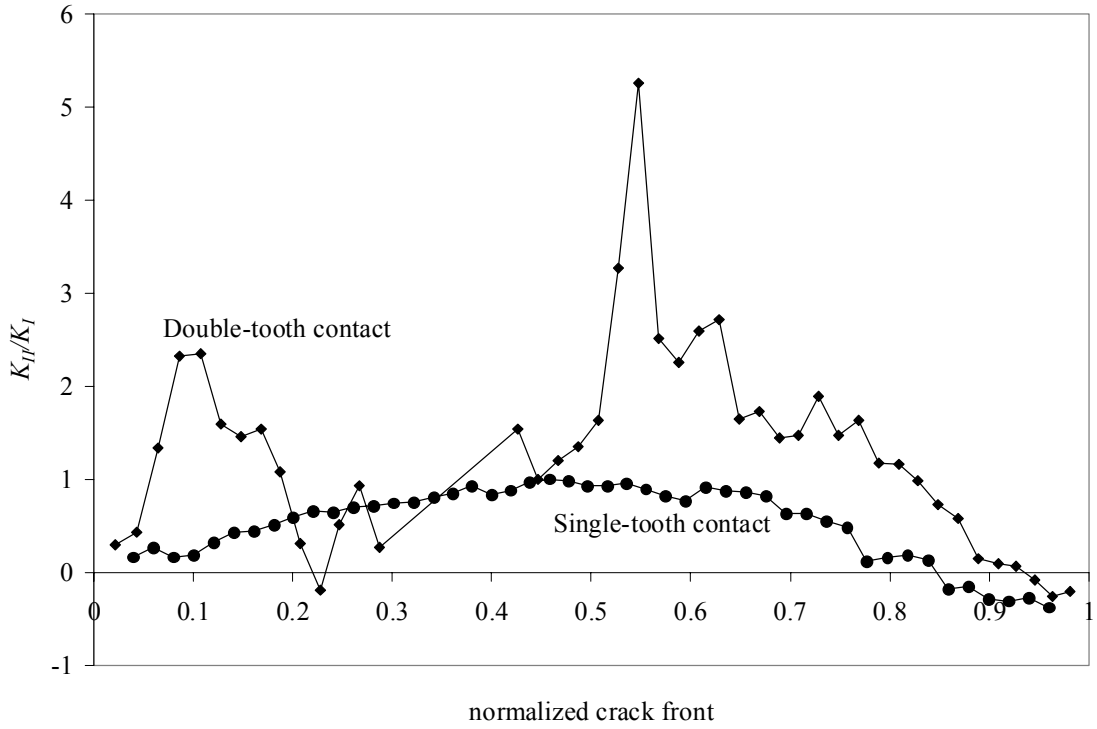

Figure 3.15: Ratio of K_{II} to K_I along the crack front for double-tooth and single-tooth contact at crack #2.

By performing these contact analyses, we were able to show that the change in the stiffness of the tooth due to a growing crack has significant effects on the SIFs and therefore on the crack trajectory and fatigue life. If LEFM analyses of section 2 are repeated under these new contact loading conditions, the change in the crack trajectory and the fatigue life of the pinion, as a result of taking into account the change in the tooth flexibility, can be determined.

4. Summary

This report summarized new results for predicting crack trajectory and fatigue life for a spiral bevel pinion using the Finite Element Method (FEM). The predictions presented in this report are based on LEFM theories combined with the FEM, incorporating plasticity induced fatigue crack closure and moving loads.

Previously in this project, three-dimensional computational simulation of crack growth in spiral bevel gears was done using BEM [1]. As a result of these analyses, a method for predicting three-dimensional, non-proportional, fatigue crack growth incorporating moving loads was developed. The BEM studies showed the need for improving the efficiency and the accuracy of the computations by employing the state-of-the-art computational capabilities.

In the current work, three-dimensional finite element modeling of the spiral bevel pinion was done using OSM/FRANC3D. A three-dimensional FEM mesh of the pinion

model was created by a 3D mesher. Moving contact loads on the tooth surface were calculated by interpolation using the shape functions on the surfaces of the loaded elements. The analyses were carried out using a parallel FEM solver, which calculates SIFs using equivalent domain J-integral method. Fatigue life predictions were made based on a modified Paris model incorporating crack closure.

In this report, we show that we can simulate fatigue crack growth in a spiral bevel gear more accurately and efficiently using the FEM along with a better representation of moving loads. Another very significant improvement was the decrease in solving time of the problem by employing parallel PC-clusters. This reduces the computation time to a few minutes while substantially increasing the resolution of the solution.

To obtain a more detailed understanding of the contact between a cracked pinion tooth in mesh with an uncracked gear tooth, three-dimensional contact analyses were performed on a spiral bevel gear set incorporating a crack. The goal in carrying out these analyses was to capture the redistribution of contact loads due to crack growth. Results of these analyses showed the expected trend of decreasing tooth loads carried by the cracked tooth with increasing crack length. We also showed that this decrease in contact loads had an impact on the SIF values and therefore would also affect the crack trajectory and fatigue life predictions.

Predicting crack trajectories more efficiently and accurately is very important for gear designers. Development of practical and accurate numerical tools for evaluating the gear performance and life enables for new and better gear designs. The work presented here provides such a tool capable of predicting crack trajectory and fatigue life in a spiral bevel gear.

Appendix: Abbreviated sample ABAQUS input file for contact analysis

```
*HEADING
FRANC3D Model
** FRANC3D Version 2.0 Generated Input File
** NUMBER OF NODES: 13029
** NUMBER OF ELEMENTS: 58712
**
** NODE DEFINITION
*NODE
1,    3.815870,    0.262049,    1.500000
2,    3.585600,    0.038081,    1.500000
3,    3.824640,    0.040620,    1.500000
.
.
.
13028,    5.109482,    0.491277,    0.734872
13029,    5.110899,    0.478949,    0.730531
** END NODE DEFINITION
**
** ELEMENT DEFINITION
*ELEMENT, TYPE=C3D4, ELSET=PID1
1,1904,1855,2100,1903
*ELEMENT, TYPE=C3D4, ELSET=PID1
2,1904,2100,1953,1952
*ELEMENT, TYPE=C3D4, ELSET=PID1
3,125,107,106,846
.
.
.
*ELEMENT, TYPE=C3D4, ELSET=PID2
58711,7717,12943,7703,13029
*ELEMENT, TYPE=C3D4, ELSET=PID2
58712,6078,7717,7703,13029
** END ELEMNT DEFINITION
**
*SOLID SECTION, ELSET=PID1, MATERIAL=MAT1
*MATERIAL, NAME=MAT1
*ELASTIC, TYPE=ISO
 3e+07, 0.3
*DENSITY
 7800
*SOLID SECTION, ELSET=PID2, MATERIAL=MAT2
*MATERIAL, NAME=MAT2
*ELASTIC, TYPE=ISO
 3e+07, 0.3
*DENSITY
 7800
**
**Definition of contact for tooth 1
**
*ELSET, ELSET=MASTER_1
26454,
26457,
26458,
.
```

```
.
.
57531,
58366,
58367,
*ELSET, ELSET=SLAVE_1
1,
2,
5,
.
.
.
22208,
24437,
24438,
*SURFACE DEFINITION, NAME=MASTER_1
26454,S4
26457,S4
26458,S4
.
.
.
57531,S1
58366,S1
58367,S1
*SURFACE DEFINITION, NAME=SLAVE_1
1,S2
2,S4
5,S4
.
.
.
22208,S1
24437,S1
24438,S1
*SURFACE INTERACTION, NAME=NOFRIC
*FRICTION
 0
*CONTACT PAIR, INTERACTION=NOFRIC
MASTER_1, SLAVE_1
**
** Definition of contact for tooth 2
**
*ELSET, ELSET=MASTER_2
26455,
26456,
26459,
.
.
.
57320,
57753,
57754,
*ELSET, ELSET=SLAVE_2
3,
4,
9,
```

```
.
.
.
24532,
24540,
24548,
*SURFACE DEFINITION, NAME=MASTER_2
26455,S4
26456,S4
26459,S4
.
.
.
57320,S1
57753,S1
57754,S1
*SURFACE DEFINITION, NAME=SLAVE_2
3,S2
4,S4
9,S4
.
.
.
24532,S1
24540,S1
24548,S1
*SURFACE INTERACTION, NAME=NOFRIC1
*FRICTION
 0
*CONTACT PAIR, INTERACTION=NOFRIC1
MASTER_2, SLAVE_2
**
** Application of displacement to ensure contact
** between gear and pinion
**
*STEP, NLGEOM, INC=100
**FRANC3D load case 1
*STATIC
1.0, 1.0
*BOUNDARY
2209,3,3, 0
2211,3,3, 0
2213,3,3, 0
2215,3,3, 0
2217,3,3, 0
2219,3,3, 0
2221,3,3, 0
2223,3,3, 0
2232,2,2, -0.01
2247,3,3, 0
.
.
.
33,1,1,0
33,2,2,0
33,3,3,0
2322,1,1,0
```

```
2322,2,2,0
2322,3,3,0
2415,1,1,0
2415,2,2,0
2415,3,3,0
*END STEP
**
** Application of full design torque
**
*STEP, NLGEOM, INC=100
**FRANC3D load case 1
*STATIC
1.0, 1.0
*BOUNDARY, OP=NEW
2209,3,3, 0
2211,3,3, 0
2213,3,3, 0
2215,3,3, 0
2217,3,3, 0
2219,3,3, 0
2221,3,3, 0
2223,3,3, 0
2247,3,3, 0
.
.
.
33,1,1,0
33,2,2,0
33,3,3,0
2322,1,1,0
2322,2,2,0
2322,3,3,0
2415,1,1,0
2415,2,2,0
2415,3,3,0
*CLOAD
2799,2,-1000
*END STEP
*STEP, NLGEOM, INC=100
**FRANC3D load case 1
*STATIC
1.0, 1.0
*CLOAD
2799,2,-3230
*FILE FORMAT, ASCII
*NODE FILE, FREQUENCY=100
U
*EL FILE, FREQUENCY=100, POSITION=NODES
S,E,PE
*RESTART,WRITE, FREQUENCY=100
*NODE PRINT, FREQUENCY=100
U
*EL PRINT, FREQUENCY=100, POSITION=NODES
*CONTACT PRINT,FREQUENCY=100
CFN,CAREA,XN
*END STEP
**END OF INPUT
```

References

[1] Spievak, L. E., Wawrzynek, P. A., Ingraffea A. R., and Lewicki, D. G. "Simulating Fatigue Crack Growth in Spiral Bevel Gears." *Engineering Fracture Mechanics* 68, no. (2001):53-76.

[2] Johnson, K. L. *Contact Mechanics*. Cambridge: Cambridge University Press, 1985.

[3] Litvin, F. L., and Zhang, Y. "Local Synthesis and Tooth Contact Analysis of Face-Milled Spiral Bevel Gears" NASA Contractor Report 4342/AVSCOM Technical Report 90-C-028, 1991.

[4] Carter, B., Chen, C-S , Chew, P., Chrisochoides, N., Gao, G.R., Heber, G., Ingraffea, A.R., Krause R., Myers, C., Nave, D., Pingali, K., Stodghill P., Vavasis, S., Wawrzynek P.A. "Parallel FEM Simulation of Crack Propagation—Challenges, Status, and Perspectives." *Lecture Notes in Computer Science* 1800, (2000):443-449.

[5] Chan S.K., Tuba I.S. and Wilson W.K. "On the finite element method in linear fracture mechanics." *Engineering Fracture Mechanics* 2, no.1, (1970): 1-17.

[6] Barsoum R.S. "On the use of isoparametric elements in linear fracture mechanics." *International Journal for Numerical Methods in Engineering* 10, (1976): 25-37.

[7] Shih C.F., deLorenzi H.G. and German M.D. "Crack extension modeling with singular quadratic isoparametric elements." *International Journal of Fracture* 12, (1976): 647-651.

[8] Ingraffea A.R. and Manu C. "Stress intensity factor computation in three dimensions with quarter-point elements." *International Journal for Numerical Methods in Engineering* 15, (1980): 1427-1445.

[9] deLorenzi H.G. "3D elastic-plastic fracture mechanics with ADINA." *International Journal of Computers and Structures* 13, (1981): 613-621.

[10] Li F.Z., Shih C.F. and Needleman A. "A comparison of methods for calculating energy release rates." *Engineering Fracture Mechanics* 21, 1985: 405-421.

[11] Shih C.F., Moran B. and Nakamura T. "Energy release rate along a three-dimensional crack front in a thermally stressed body." *International Journal of Fracture* 30, (1986): 79-102.

[12] Moran B. and Shih C.F. "A general treatment crack tip contour integrals." *International Journal of Fracture* 35, (1987): 295-310.

[13] Moran B. and Shih C.F. "Crack tip and associated domain integrals from momentum and energy balance." *Engineering Fracture Mechanics* 27, no.6, (1987): 615-642.

[14] Dodds Jr., R.H. and Vargas, P.M. "Numerical evaluation of domain and contour integrals for nonlinear fracture mechanics: formulation and implementation aspects." Report, University of Illinois at Urbana-Champaign, Department of Civil Engineering, 1988.

[15] Rice J.R. "A path independent integral and the approximate analysis of strain concentration by notches and cracks." *Journal of Applied Mechanics*, 35 (1968): 379-386.

[16] Bui H.D. “Associated path independent J-integrals for separating mixed modes.” *Journal of the Mechanics and Physics of Solids* 31, no.6, (1983): 439-448.

[17] Nikishov G. P. and Atluri S.N. “Calculation of fracture mechanics parameters for an arbitrary three-dimensional crack, by the ‘Equivalent Domain Integral’ method.” *International Journal for Numerical Methods in Engineering* 24, no.9 (1987): 1801-1821.

[18] Chen K.L., and Atluri S.N. “Comparison of different methods of evaluation of weight functions for 2D mixed-mode fracture analysis.” *Engineering Fracture Mechanics* 34, no.4 (1989): 935-956.

[19] Murakami Y. (Editor-in-Chief) Stress Intensity Factors Handbook. Pergamon Press, (1987).

[20] Bibel, G.D., Kumar, A., Reddy, S., and Handschuh, R. “Contact stress analysis of spiral bevel gears using finite element analysis.” *Journal of Mechanical Design* 117, no.2A (1995): 235-240.

[21] Bibel, G.D., and Handschuh, R. “Meshing of a Spiral Bevel Gearset with 3D Finite Element Analysis.” NASA Technical Report ARL-TR-1224 (1996).

[22] Handschuh, R.F., and Bibel, G.D. “Comparison of experimental and analytical tooth bending stress of aerospace spiral bevel gears.” NASA Technical Report ARL-TR-1891 (1999).

[23] Vijakaar, S. “A combined surface integral and finite element solution for a three-dimensional contact problem.” *International Journal for Numerical Methods in Engineering* 31, no. (1991): 525-545.

[24] ABAQUS/Standard, Version 6.1.1, Hibbitt, Karlsson & Sorensen Inc.

REPORT DOCUMENTATION PAGE

Form Approved
OMB No. 0704-0188

1. AGENCY USE ONLY (*Leave blank*)	2. REPORT DATE	3. REPORT TYPE AND DATES COVERED
	August 2003	Final Contractor Report

4. TITLE AND SUBTITLE

Simulating Fatigue Crack Growth in Spiral Bevel Pinion

5. FUNDING NUMBERS

WBS–22–708–90–01
NAS3–1993
L162211A47A

6. AUTHOR(S)

Ani Ural, Paul A. Wawrzynek, and Anthony R. Ingraffea

7. PERFORMING ORGANIZATION NAME(S) AND ADDRESS(ES)

Cornell University
Cornell Fracture Group
Rhodes Hall
Ithaca, New York 14850

8. PERFORMING ORGANIZATION REPORT NUMBER

E–14091

9. SPONSORING/MONITORING AGENCY NAME(S) AND ADDRESS(ES)

National Aeronautics and Space Administration
Washington, DC 20546–0001
and
U.S. Army Research Laboratory
Adelphi, Maryland 20783–1145

10. SPONSORING/MONITORING AGENCY REPORT NUMBER

NASA CR—2003-212529
ARL–CR–0531

11. SUPPLEMENTARY NOTES

Project Manager, David Lewicki, Structures and Acoustics Division, NASA Glenn Research Center, organization code 5950, 216–433–3970.

12a. DISTRIBUTION/AVAILABILITY STATEMENT

Unclassified - Unlimited
Subject Category: 37 Distribution: Nonstandard

Available electronically at http://gltrs.grc.nasa.gov

This publication is available from the NASA Center for AeroSpace Information, 301–621–0390.

12b. DISTRIBUTION CODE

13. ABSTRACT ***(Maximum 200 words)***

New results for predicting crack trajectory and fatigue life for a spiral bevel pinion using the Finite Element Method (FEM) are reported. The predictions presented are based on linear elastic fracture mechanics combined with the FEM, incorporating plasticity induced fatigue crack closure and moving gear tooth loads. The analyses were carried out using a parallel FEM solver, which calculates stress intensity factors using equivalent domain J-integral method. Fatigue life predictions were made based on a modified Paris model incorporating crack closure. To obtain a more detailed understanding of the contact between a cracked pinion tooth in mesh with an uncracked gear tooth, three-dimensional contact analyses were performed on a spiral bevel gear set incorporating a crack. The goal in carrying out these analyses was to capture the redistribution of contact loads due to crack growth. Results of these analyses showed the expected trend of decreasing tooth loads carried by the cracked tooth with increasing crack length. It was also showed that this decrease in contact loads had an impact on the stress intensity factor values and therefore would also affect the crack trajectory and fatigue life predictions.

14. SUBJECT TERMS

Spiral-bevel gears; Cracks; Finite element analysis; Boundary element analysis; Fracture mechanics; Stress intensity factors; Contact analysis

15. NUMBER OF PAGES

48

16. PRICE CODE

17. SECURITY CLASSIFICATION OF REPORT	18. SECURITY CLASSIFICATION OF THIS PAGE	19. SECURITY CLASSIFICATION OF ABSTRACT	20. LIMITATION OF ABSTRACT
Unclassified	Unclassified	Unclassified	